

Article

# Vis-Responsive Copper-Modified Titania for Decomposition of Organic Compounds and Microorganisms

Maya Endo-Kimura <sup>1</sup>, Bariş Karabiyik <sup>1</sup>, Kunlei Wang <sup>1,2</sup> , Zhishun Wei <sup>3</sup> , Bunsho Ohtani <sup>1</sup> , Agata Markowska-Szczupak <sup>4</sup> and Ewa Kowalska <sup>1,\*</sup> 

- <sup>1</sup> Institute for Catalysis, Hokkaido University, N21, W10, Sapporo 001-0021, Japan; m\_endo@cat.hokudai.ac.jp (M.E.-K.); bakarabiyik@gmail.com (B.K.); kunlei@cat.hokudai.ac.jp (K.W.); ohtani@cat.hokudai.ac.jp (B.O.)
- <sup>2</sup> Northwest Research Institute, Co., Ltd. of C.R.E.C., Lanzhou 730099, China
- <sup>3</sup> Hubei Provincial Key Laboratory of Green Materials for Light Industry, Hubei University of Technology, Wuhan 430068, China; wei.zhishun@hbut.edu.cn
- <sup>4</sup> Department of Chemical and Process Engineering, West Pomeranian University of Technology in Szczecin, Piastów 42, 71-065 Szczecin, Poland; Agata.Markowska@zut.edu.pl
- \* Correspondence: kowalska@cat.hokudai.ac.jp; Tel.: +81-11-706-9130

Received: 19 September 2020; Accepted: 14 October 2020; Published: 16 October 2020



**Abstract:** Seven commercial titania (titanium(IV) oxide; TiO<sub>2</sub>) powders with different structural properties and crystalline compositions (anatase/rutile) were modified with copper by two variants of a photodeposition method, i.e., methanol dehydrogenation and water oxidation. The samples were characterized by diffuse reflectance spectroscopy (DRS), X-ray powder diffraction (XRD), scanning electron microscopy (SEM), energy-dispersive X-ray spectroscopy (EDS) and X-ray photoelectron spectroscopy (XPS). Although zero-valent copper was deposited on the surface of titania, oxidized forms of copper, post-formed in ambient conditions, were also detected in dried samples. All samples could absorb visible light (vis), due to localized surface plasmon resonance (LSPR) of zero-valent copper and by other copper species, including Cu<sub>2</sub>O, CuO and Cu<sub>x</sub>O (x:1-2). The photocatalytic activities of samples were investigated under both ultraviolet (UV) and visible light irradiation (>450 nm) for oxidative decomposition of acetic acid. It was found that titania modification with copper significantly enhanced the photocatalytic activity, especially for anatase samples. The prolonged irradiation (from 1 to 5 h) during samples' preparation resulted in aggregation of copper deposits, thus being detrimental for vis activity. It is proposed that oxidized forms of copper are more active under vis irradiation than plasmonic one. Antimicrobial properties against bacteria (*Escherichia coli*) and fungi (*Aspergillus niger*) under vis irradiation and in the dark confirmed that Cu/TiO<sub>2</sub> exhibits a high antibacterial effect, mainly due to the intrinsic activity of copper species.

**Keywords:** copper-modified titania; plasmonic photocatalysts; heterogeneous photocatalysis; bactericidal activity; antifungal effect

## 1. Introduction

Titania (TiO<sub>2</sub>) is one of the most widely investigated semiconductor photocatalysts because it is abundant, cost-effective, highly active, and environmentally friendly. Furthermore, titania has high photocatalytic activity and good chemical and thermal stability [1–3]. Therefore, it has been broadly used for water and wastewater treatment, air purification and energy conversion [1,4–8]. The crystalline form (i.e., anatase, rutile and brookite), the surface properties (e.g., specific surface area, crystallinity and crystallite size) and the morphology of titania photocatalysts govern the photocatalytic

performance. For example, detailed study of commercial titania P25 photocatalyst, which contains anatase, rutile and non-crystallite phase, has revealed that the superiority of anatase or rutile depends on the photocatalytic reaction system, i.e., anatase is more active for oxidative decomposition of organic compounds, whereas rutile is more efficient for methanol dehydrogenation [9]. Although titania photocatalysts are considered as highly active, the charge carriers' recombination (typical for all semiconductors) results in lower quantum yields of photocatalytic reaction than expected 100%. Accordingly, various studies on activity enhancement have been performed, including also the morphology architecture, and thus titania in the form of nanowires, nanoflakes, nanotubes, nanorods, mesocrystals, mesoporous networks (aerogels) and as faceted nanoparticles have been intensively investigated [10–15]. For example, titania nanorods have shown higher activity than both nanoparticles and nanospheres in the degradation of dye, probably due to the nanoporous structure, which might allow an effective transport of the reactant molecules to the active sites [13].

There are two main mechanisms of organic compounds' decomposition during photocatalytic degradation, i.e., (i) direct reaction of a substrate with photo-generated charge carriers on the photocatalyst surface, and (ii) indirect reaction with reactive oxygen species (ROS), generated from oxygen and water. In situ Fourier transform infrared (FT-IR) study has elucidated that 4-chlorophenol degradation occurs both on the surface of titania, and by the reductive dechlorination proceeds by superoxide anion radical ( $O_2^-$ ) [16], and thus it is proposed that the affinity of titania surface to a substrate is crucial for the effectiveness of photocatalytic degradation [16,17]. Recently, the complete decomposition of pollutants, such as organic compounds and textile dyes, has been reported for a variety of modified titania photocatalysts under ultraviolet (UV) irradiation [18–20].

However, as titania absorbs only UV light and the solar spectrum contains just 3–4% of UV, only a small portion of the incident solar energy is utilized by conventional titania photocatalysts [21], thus limiting their reactivity. Consequently, there is great interest in modification of titania to extend the onset of absorption into the visible (vis) region of solar spectrum. The methods of titania modification include: (i) doping with non-metals [22–25], (ii) coupling with narrower-bandgap semiconductors [26–29], (iii) preparation of oxygen-deficient titania ("self-doped") [30], and (iv) various kinds of surface modifications, e.g., with nanoparticles/nanoclusters of metals [31–35], metal complexes [36,37], anions (e.g., surface fluorination [38]), metal cations and their oxides (e.g., Co, Cr, Cu, Fe, Mo, V, and W [39], Li and rare-earth elements [40]), carbon-containing compounds (e.g., alcohols [41], glucose [42], graphene [43]). It might be concluded that the surface modification has been more intensively studied and recommended since doping might generate recombination centers in the crystal structure (dopants as recombination centers), resulting in a decrease in photocatalytic activity under UV irradiation [44].

Since the pioneering work of Bard in 1978 [31], noble metals have played the leading role among available surface modifiers since not only do they shift photoactivation towards vis response, but they also enhance photocatalytic activity under UV irradiation. Noble-metal-loading provides chemically active sites, and thus metal deposits lower the activation barrier and prevent charge carriers' recombination by formation of a Schottky barrier (resulting from higher work function of metals than electron affinity of  $TiO_2$ ) increasing the transfer of photoexcited electrons to the substrates under UV illumination. Although activity enhancement for titania (and other semiconductors) under UV irradiation has been well known for about 50 years, activation of wide-bandgap semiconductors at vis range by noble metals has been investigated in the last decade [44–46]. Despite the precise mechanism of vis activity remaining unclarified (whether through energy transfer, electron transfer or plasmonic heating), it is apparent that surface plasmon resonance (SPR) of noble metals is responsible for this phenomenon [47]. SPR, the collective oscillation of the valence electrons, is induced when the frequency of photons matches the frequency of the surface electrons. The plasmon wavelength depends on the nature of the metal and the properties of metallic deposits, such as the size and the shape [48,49]. Hence, the entire solar spectrum might be used by the proper design of the composition and the morphology of plasmonic nanostructures [48,50–54]. Light below the plasmon frequency is

reflected (screening of electric field of light) and above is transmitted (electrons cannot respond fast enough) [55]. Moreover, the energetic charge carriers might release the energy by converting it to local thermal energy or by transferring it to the surroundings [56,57].

In addition to the photocatalytic properties of titania for degradation of organic compounds and energy conversion, titania has also been proposed as an antimicrobial agent after an initial report by Matsunaga et al. in 1985 [58]. Since then, many studies have been performed and titania has been shown to inhibit bacteria, fungi, viruses and protozoa. Accordingly, titania might be used as an effective disinfectant for air, water and various surfaces (e.g., tables, walls and medical devices) [59–65]. The recent study has mainly focused on solar disinfection (SODIS), which indicates that titania (and other semiconductor photocatalysts) significantly enhance the overall disinfection rate [66]. Although many reports on SODIS have been published, including mechanistic studies, e.g., the combined effect of heating and generation of ROS under UV irradiation [67], a lack of knowledge about the mechanism of titania-based photocatalysis under vis conditions remains. Thus, effective design of photoactive materials with optimal antimicrobial activity under solar radiation continues to prove elusive [68].

Copper (Cu) is considered as an excellent environmental purifier due to its attractive cost (in comparison to other noble metals), low toxicity for humans and high antimicrobial activity. It has been proposed that the bactericidal mechanisms of copper involve adsorption of Cu ions on the surface of bacteria, and then (1) the surface proteins are denatured [69], and/or (2) adsorbed Cu ions induce oxidative stress [70]. Furthermore, it has been reported that Cu<sub>2</sub>O has higher activity in inactivation of bacteria than CuO and Ag [69]. On the other hand, Cu nanoparticles (NPs) have lower toxicity than Ag NPs against some species of fungi [71]. It has also been revealed that copper-modified titania photocatalysts show high antimicrobial efficiency [72,73]. It is believed that modification of titania with small amount of an inexpensive noble metal (Cu) would result in preparation of environmentally friendly materials with high levels of activity. However, it is also known that the properties of photocatalysts govern the overall activity. Accordingly, in this study, Cu NPs have been deposited on various commercial titania photocatalysts under different preparation conditions, and investigated for the photocatalytic decomposition of the organic compounds (acetic acid and methanol) and microorganisms (bacteria and fungi) in order to clarify the property-governed activity.

## 2. Results and Discussion

### 2.1. Preparation of Cu-Modified Titania

In this study, seven commercial titania samples, i.e., ST-01, FP6, P25, ST-41, TIO-6, ST-G1 and TIO-5, have been used, and their properties are shown in Table 1.

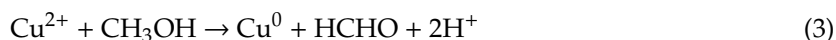
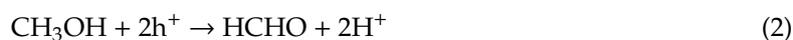
**Table 1.** The characteristics of commercial titania samples.

Titania	Crystalline Form <sup>I</sup> (A%) <sup>II</sup>	Crystallite Size <sup>III</sup> (nm)	SSA <sup>III</sup> (m <sup>2</sup> g <sup>-1</sup> )	ETs <sup>III</sup> (μmol g <sup>-1</sup> )
ST-01	A (100)	8	298	84
FP6	A/R (92.5)	15	103.7 <sup>IV</sup>	154 <sup>IV</sup>
P25	A/R (84.8)	28	59	50
ST-41	A/R (99.7)	208	11	25
TIO-6	R (0)	15	100	242
ST-G1	R/A (1.9)	205	5.7	50
TIO-5	R/A (8.6)	570	3	14

<sup>I</sup> A: anatase, R: rutile, A/R and R/A: mixture with majority of anatase and rutile, respectively. <sup>II</sup> The content of anatase (without consideration of non-crystalline phase, i.e., [A]% + [R]% = 100%). <sup>III</sup> data reported previously (except for FP6) in [74] and <sup>IV</sup> FP6 in [75], SSA—specific surface area, ETs—density of defective sites (electron traps).

Copper was photodeposited on titania in two reaction systems, i.e., during dehydrogenation of methanol, and water oxidation. The reactions occurring during Cu deposition can be presented by Equations (1)–(2) and (4)–(5), respectively, and summarized by Equations (3) and (6), as shown below:

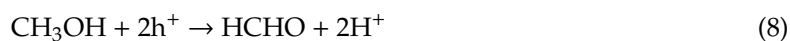
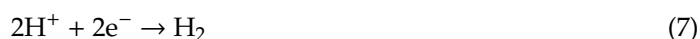
(i) during methanol dehydrogenation (Equations (1)–(3)):



(ii) during water oxidation (Equations (4)–(6)):



In the case of methanol dehydrogenation, the formation of metallic deposits on the titania surface (here zero-valent Cu) results in the evolution of hydrogen ( $\text{H}_2$ ), as Cu (similar to other noble metals) works as a co-catalyst on which molecular hydrogen is formed (negligible activity of titania without co-catalyst for alcohol dehydrogenation), as follows (Equations (7) and (8), and summarized as Equation (9)):



The obtained results of methanol dehydrogenation and water oxidation during Cu NPs formation are shown in Figure 1. It was found that the ST-01 sample (fine anatase) was the most active, reaching an approximately 10-fold higher rate of  $\text{H}_2$  evolution than other titania samples, especially during the first hour of irradiation (Figure 1a). Almost all samples (except TIO-6) show good linearity in  $\text{H}_2$  generation after 30 min of irradiation (induction time for formation of Cu NPs), indicating that 30 min could be sufficient for complete deposition of Cu in methanol solution. On the other hand, the efficiency of water oxidation is low, and only slightly linear evolution of oxygen was observed for TIO-6 sample (fine rutile), as shown in Figure 1b. It is thought that water oxidation is not effective, probably because copper is less noble than platinum and gold, and thus easily oxidizable in water and air. Indeed, there are no other reports on Cu for photocatalytic water oxidation.

Almost linear evolution of hydrogen has been observed for all samples (except TIO-6; probably due to the largest content of electron traps slowing down the copper deposition) during 1 h irradiation (Figure 1a) in methanol. Prolonged irradiation (up to 5 h) has also been applied to check how and if the properties of obtained samples differ, and the data of  $\text{H}_2$ -evolution rate are shown in Figure 1c. Similar to 1 h photodeposition, the ST-01 sample shows the highest efficiency for methanol dehydrogenation, which is not surprising as large specific surface area has been reported to be a key-factor of hydrogen evolution for anatase-based titania, e.g., in the case of gold- [44], silver- [76] and platinum- [77] modified titania samples. Although quite good linearity in  $\text{H}_2$  evolution was observed after 30 min of irradiation (Figure 1a), the data for prolonged irradiation indicate that at least 1 h of irradiation is necessary to ensure complete deposition of copper (linear evolution of  $\text{H}_2$  starting at about 1 h).

Moreover, the efficiencies of anatase are higher than rutile for  $\text{H}_2$  evolution (methanol dehydrogenation), whereas rutile-containing photocatalysts are more active than anatase ones for  $\text{O}_2$  evolution, probably due to the smaller Ti–Ti distance in rutile than that in anatase, leading to the formation of a surface structures, such as Ti–OO–Ti [78], and thus enhanced evolution of  $\text{O}_2$ . Hence, the photocatalytic activity during Cu-photodeposition corresponded to the findings by Buchalska et al. showing that rutile is an active phase in reduction reactions (by photogenerated electrons), whereas anatase in oxidation reactions (by photogenerated holes) [79].

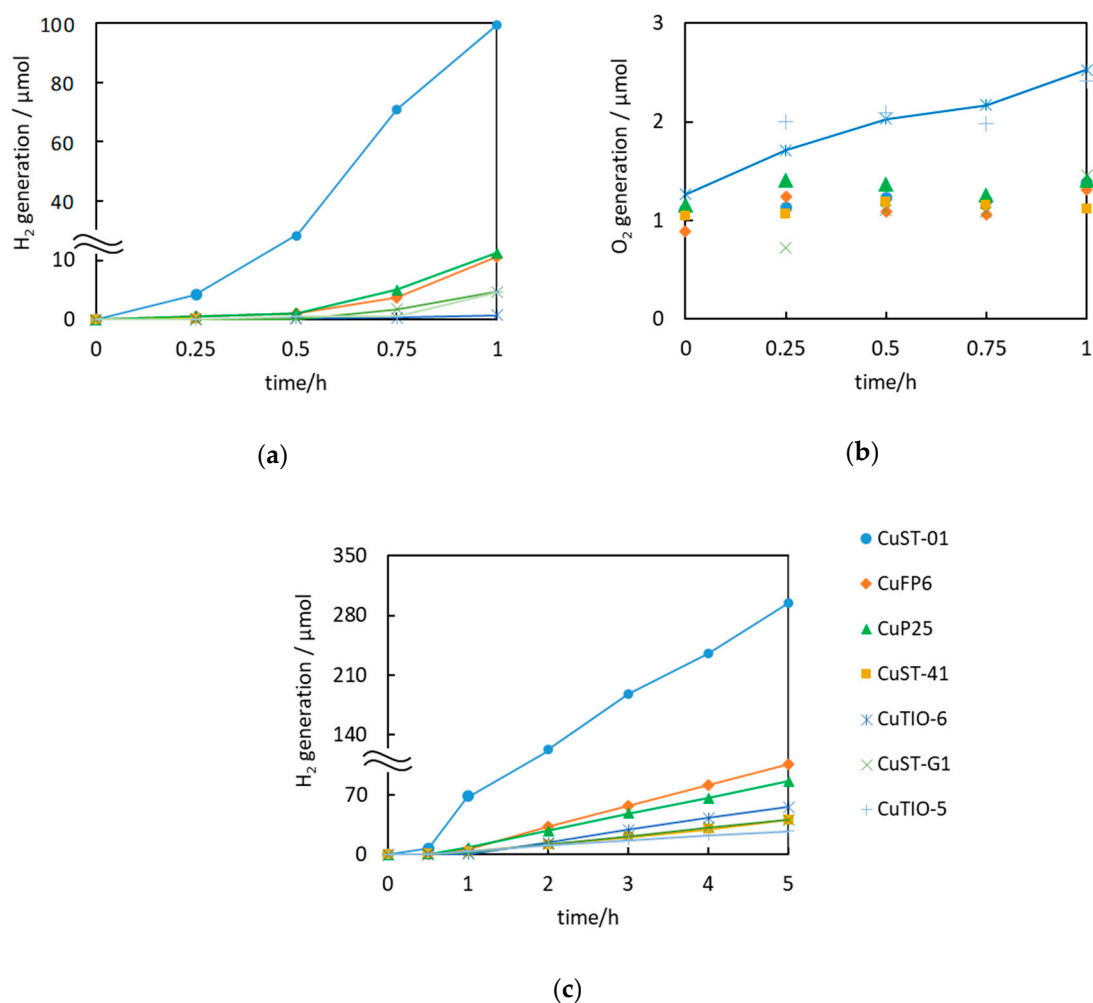


**Figure 1.** Hydrogen and oxygen evolution during the photodeposition of copper on titania: (a) in methanol/water for 1 h, (b) in water for 1 h, (c) in methanol/water for 5 h.

## 2.2. Photoabsorption Properties (Ultraviolet-Visible (UV-Vis) Diffuse Reflectance Spectroscopy)

The modification of titania with copper causes its coloration, i.e., color change from white into light green-blue for anatase-rich samples of fine particles (ST-01, FP6 and P25), light green for the fine rutile sample (TIO-6) and light grey for titania samples with large particles (ST-41, ST-G1 and TIO-5), as shown in the insets of Figure 2. The greyish color of large titania samples indicates the polydispersity of deposited copper NPs, similar to reported gold-modified titania samples (Although usually violet/pink samples are obtained, photodeposition of gold on large rutile results in greyish coloration because of high polydispersity of gold deposits, i.e., both size and shape of NPs, nanorods and irregularly-shaped deposits, and thus broad localized-surface plasmon resonance (LSPR) peak [44]). It has been proposed that noble metals are mainly deposited on surface defects [80], and since fine titania contains large content of defects (Table 1, ETs [77]), fine noble-metal NPs are formed and uniformly deposited on the titania surface [44]. In contrast, in the case of well-crystallized large titania samples, a low content of defects (Table 1, [77]) results in aggregation of noble-metal NPs, and thus larger NPs and with various shapes are finally deposited on the surface of large titania samples [44]. The green-blue color of Cu-modified titania has commonly been reported, indicating the possible presence of mixed-oxidation state of copper (Cu(II), Cu(I), Cu(0) and Cu<sub>x</sub>O for x = 1–2) [72,81–83].

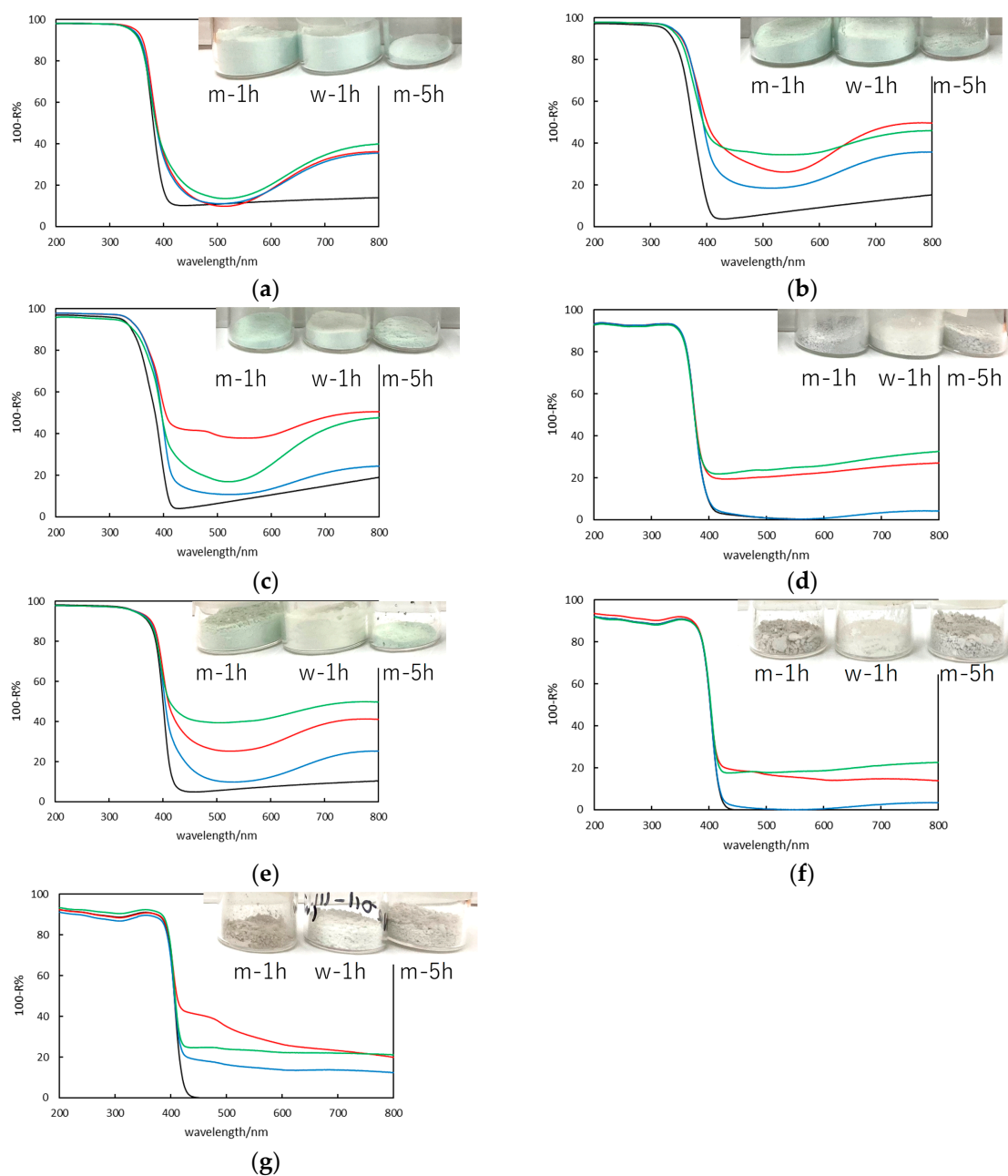


**Figure 2.** Diffuse reflectance (DR) spectra with respective photographs of copper-modified titania (with diffuse reflectance spectroscopy (DRS) for bare titania as reference): (a) ST-01, (b) FP6, (c) P25, (d) ST-41, (e) TIO-6, (f) ST-G1 and (g) TIO-5 (black: bare, red: m-1h, blue: w-1h, green: m-5h).

Indeed, the absorption spectra confirm the possibility of co-existence of different copper forms, as shown in Figure 2. The typical absorption of zero-valent Cu (due to LSPR), interband absorption of  $\text{Cu}_2\text{O}$ , and intrinsic exciton  $\text{CuO}$  and/or d-d transition of  $\text{Cu}^{2+}$  are expected at about 570, 500–600, and 600–800 nm, respectively [72,84,85]. Moreover, the clear absorption in the range of 400–500 nm, especially for fine titania samples (Figure 2a–c,e) might be caused by the interfacial charge transfer (IFCT) from the valence band (VB) of  $\text{TiO}_2$  to  $\text{Cu}_x\text{O}$  clusters [86]. Interestingly, very similar photoabsorption properties have been obtained for ST-01-based samples, independently on the preparation conditions (Figure 2a), i.e., with clear interfacial charge transfer ( $\text{Cu}_x\text{O}/\text{TiO}_2$ ) between 400 and 500 nm and intrinsic exciton of  $\text{CuO}$  and/or d-d transition of  $\text{Cu}^{2+}$ , suggesting that oxidized forms of copper are predominant in these samples. Furthermore, the  $\text{CuST-01w-1h}$  sample exhibits the lowest absorption

at 570 nm, and thus the lack of zero-valent copper in this sample is expected as a result of its preparation in the presence of oxygen ( $O_2$  evolution). It has been reported that even in deaerated methanol solution, although zero-valent copper is formed and deposited on titania (violet coloration of suspension during photodeposition), copper is further oxidized easily during sample washing and drying, forming mixed-oxidation-state deposits, possibly the metallic core and oxidized shell [81,82]. Interestingly, the absorption spectra of Cu/FP6 samples indicate the possibility of co-presence of zero-valent copper because of stronger absorption at about 570 nm than that for a bare titania sample, especially for CuFP6m-5h. Unfortunately, no clear LSPR peak could be seen, probably because of peak damping caused by interband transition of CuO [49]. In contrast, in the case of Cu/P25 samples, shorter irradiation in reductive conditions (m) results in stronger photoabsorption at LSPR range, as shown in Figure 2c. In the case of large anatase (ST-41), samples prepared in methanol have almost the same photoabsorption properties until 600 nm, and prolonged irradiation results in stronger “absorption”, which could be caused by light scattering on larger NPs (Figure 2d). It is expected that prolonged photodeposition might result in aggregation of copper deposits since it is carried out under continuous stirring allowing an easy contact between deposits (similar aggregation has been observed for gold-modified titania during long-term irradiation, especially for large titania samples (unpublished data)). Indeed, all samples prepared during 5 h irradiation (green lines) show a continuous increase in photoabsorption with an increase in wavelengths, indicating enhanced scattering on larger copper deposits, which is clearly seen especially for large titania samples. In the case of fine rutile samples (TIO-6), similar spectra to that by fine anatase samples have been obtained, indicating the co-presence of various forms of copper, predominantly in oxidized state (Figure 2e). In the case of large rutile samples (ST-G1 and TIO-5), the photoabsorption spectra correlate with those of large anatase, and no clear absorption peaks could be determined, well-corresponding with greyish color of samples (absorption at whole vis range). Interestingly, in the case of P25 and ST-G1 samples modified with copper during 1 h irradiation in methanol (red lines), clear peaks at about 470 nm could be seen, corresponding to the  $Cu_2O$  presence, as also confirmed by X-ray diffraction (XRD) and X-ray photoelectron spectroscopy (XPS) analysis (discussed further).

### 2.3. X-Ray Diffraction

The presence of copper has been confirmed in all samples by X-ray diffraction, as summarized in Table 2 and shown in Figure 3. In the case of fine titania particles, titania peaks are very broad and thus overlapping with copper ones. Accordingly, Rietveld refinement has been used for peaks' separation. It should be pointed out that titania peaks do not change after copper photodeposition (i.e., shift, broadening), confirming that surface modification does not influence the crystalline properties of titania. Although for ST-01 and P25 samples clear peaks of copper could be hardly seen, XRD patterns for other samples, especially those prepared in methanol, prove the copper presence (as zero-valent or  $Cu_2O$ ), as shown in Figure 3b,d–g. As expected, usually larger content of crystalline cuprous oxide has been obtained in samples prepared during water oxidation than that during methanol dehydrogenation. Moreover, longer irradiation in methanol causes the preparation of samples with larger content of zero-valent copper, with the exception of very fine titania (FP6 and TIO-6), which could be caused by formation of very fine Cu NPs, and thus easily oxidizable (whole NPs) in air, whereas larger Cu NPs are only partly oxidized (surface as a shell) keeping zero-valent core. The larger content of deposited copper, and especially zero-valent copper during longer irradiation time might be caused by: (i) its more efficient reduction, and thus complete deposition of copper on titania, and (ii) aggregation of copper NPs, causing partial stabilization of zero-valent copper inside these aggregates. Moreover, the largest content of zero-valent copper has been obtained for large titania NPs, i.e., ST-41, ST-G1 and TIO-5 (and thus with large copper NPs) and for the finest titania (ST-01), which could confirm the stabilization of zero-valent copper either as a core of larger particles ( $Cu@Cu_xO$ ) or densely surrounded by fine titania (similar to zero-valent copper placed in titania aerogel nanostructure [82]), respectively. Moreover, it has been confirmed (according to diffuse reflectance (DR) spectra) that larger crystals have

been formed on larger titania NPs due to the lower content of surface defects, as already found for gold-modified titania samples [44].

**Table 2.** The crystalline properties of Cu-modified titania by XRD measurement.

Titania		Crystalline Content/%				Crystallite Size/nm			
		Anatase	Rutile	Cu	Cu <sub>2</sub> O	Anatase	Rutile	Cu	Cu <sub>2</sub> O
ST-01	m-1h	98.0	0	1.3	0.7	8.5	ND	8.6	8.6
	w-1h	99.7	0	0.01	0.3	8.5	ND	ND	0.7
	m-5h	96.9	0	2.4	0.7	8.3	ND	1.9	0.7
FP6	m-1h	92.0	7.0	0.2	0.8	12.5	12.0	12.3	9.7
	w-1h	90.9	7.0	1.7	0.5	12.6	11.1	11.3	15.6
	m-5h	93.9	5.8	0.1	0.2	12.3	14.7	9.3	9.2
P25	m-1h	81.6	16.7	0.4	1.4	23.2	38.8	2.4	2.9
	w-1h	82.9	16.1	0.1	0.9	22.9	41.2	10.2	11.2
	m-5h	83.6	15.5	0.8	0.15	22.9	44.6	10.1	4.6
ST-41	m-1h	95.7	3.3	0.5	0.5	80.8	12.0	40.3	34.9
	w-1h	98.3	0.9	0.4	0.4	78.3	57.3	14.9	17.0
	m-5h	96.8	1.6	1.0	0.7	81.1	36.9	68.2	32.6
TIO-6	m-1h	0	97.5	2.5	0	ND	18.8	8.2	ND
	w-1h	0	97.5	2.5	0	ND	19.3	4.2	ND
	m-5h	0.8	97.3	0.1	1.8	7.5	19.0	22.2	0.7
ST-G1	m-1h	0.9	97.6	0.2	1.3	20.7	87.1	46.3	71.7
	w-1h	1.2	98.6	0.02	0.1	46.7	93.8	ND	74.1
	m-5h	0.2	98.1	0.9	0.9	20.0	95.5	51.4	3.6
TIO-5	m-1h	8.9	90.0	0	1.1	152.1	168.6	5.2	42.7
	w-1h	4.3	94.2	0.1	1.5	147.1	157.2	58.3	13.3
	m-5h	8.9	89.2	0.8	1.1	169.5	197.6	36.8	66.6

It should be pointed out that although cupric oxide has not been detected, the oxidation of zero-valent copper and cuprous oxide is highly possible (considering DRS and XPS data, and previous studies). It is thought that CuO might predominantly exist as an amorphous form rather than a crystalline one since samples have not been calcined after preparation. In the case of large titania particles, clear Cu and Cu<sub>2</sub>O peak could be observed in XRD patterns, as shown in Figure 3d,f,g. Interestingly, the clear photoabsorption peak of Cu<sub>2</sub>O at about 470 nm for CuP25m-1h and CuTIO-5m-1h (red lines in Figure 2c,g) correlates well with its largest content in those samples.

#### 2.4. Scanning Electron Microscopy

The morphology of samples has been investigated by scanning electron microscopy (SEM) observation. It has been confirmed that the properties of copper NPs depend on the properties of TiO<sub>2</sub> particles (Figure 4a–d), as suggested from DR spectra. Indeed, although Cu NPs on fine TiO<sub>2</sub> particles (ST-01, FP6, TIO-6) are hardly detected due to nano-sized nature (Figure 4a), relatively large Cu NPs are observed in the case of prolonged irradiation (CuTIO-6m-5h, Figure 4b), possibly due to the aggregation of Cu NPs during long-term stirring. In contrast, clear Cu deposits are seen on large TiO<sub>2</sub> particles (ST-41, ST-G1 and TIO-5), as shown for CuTIO-5m-1h and 5h sample in Figure 4c,d. Copper NPs have aggregated forming large particles (>100 nm) on the surface of large titania crystals (TIO-5). Moreover, although a large number of fine Cu NPs (of several nanometers) are clearly observed in CuTIO-5m-1h sample (in addition to large NPs), fine NPs have almost disappeared in the CuTIO-5m-5h sample, confirming that longer stirring during sample preparation results in NP aggregation. Energy-dispersive X-ray spectra of Cu-modified titania samples are shown (with corresponding SEM images) in Figure 4c,d for CuST-01m-5h and CuST-41m-5h samples, respectively. Although, CuSO<sub>4</sub> has been used as a copper source, sulfur has not been detected in analyzed samples, confirming efficient sample washing after copper photodeposition. The estimated content of copper

on fine (ST-01) and large (ST-41) anatase samples prepared during 5 h irradiation in methanol differs slightly from expected value (2 wt%), reaching 1.22 wt% and 2.60 wt%, respectively.

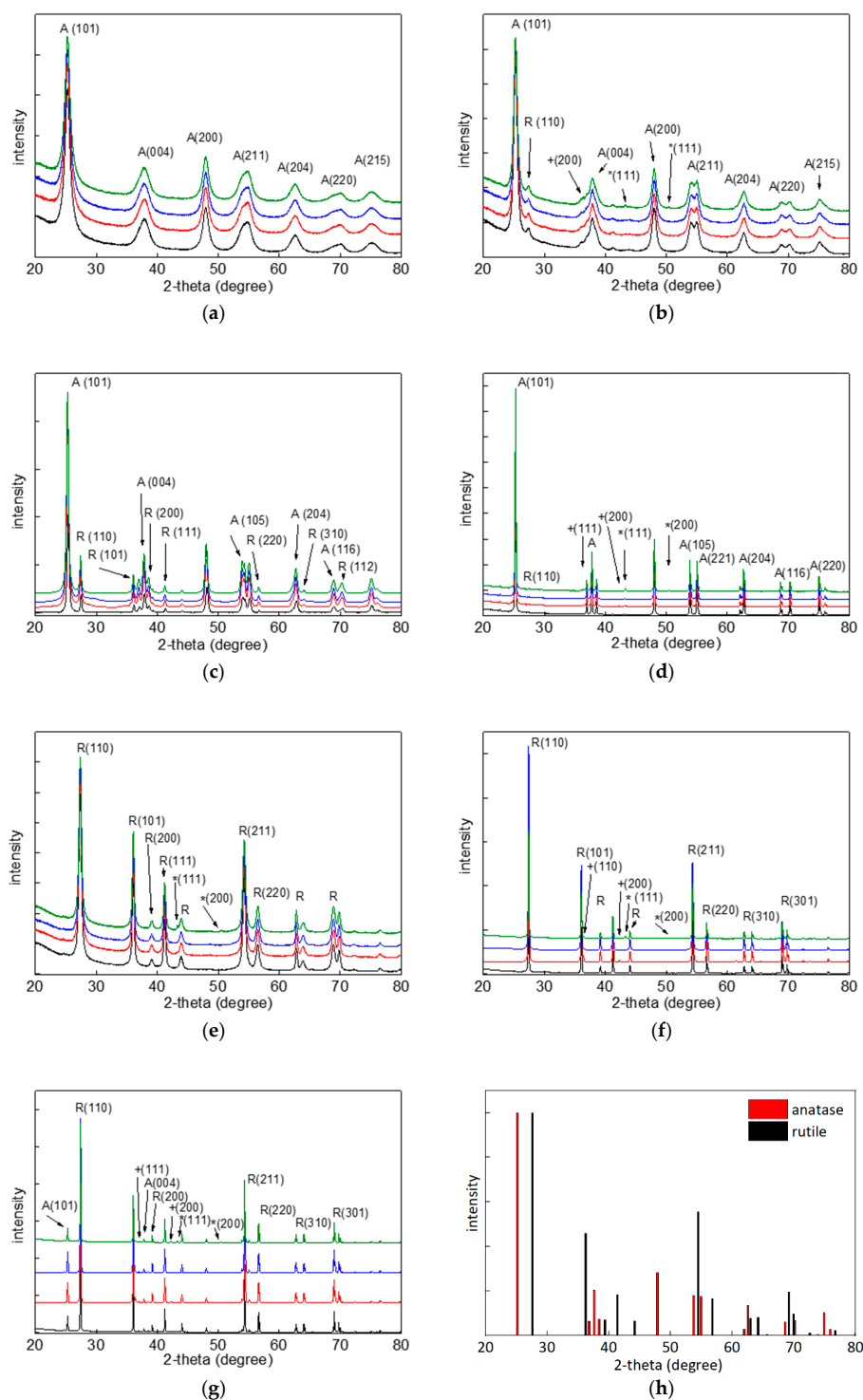


**Figure 3.** X-ray diffraction (XRD) patterns of: (a–g) bare and copper-modified TiO<sub>2</sub>: (a) ST-01, (b) FP6, (c) P25, (d) ST-41, (e) TIO-6, (f) ST-G1 and (g) TIO-5 (black: bare, red: m-1h, blue: w-1h, green: m-5h); A and R indicate anatase and rutile, respectively; Symbols (\* and +) indicate Cu and Cu<sub>2</sub>O, respectively; (h) standard XRD patterns of anatase (red) and rutile (black).

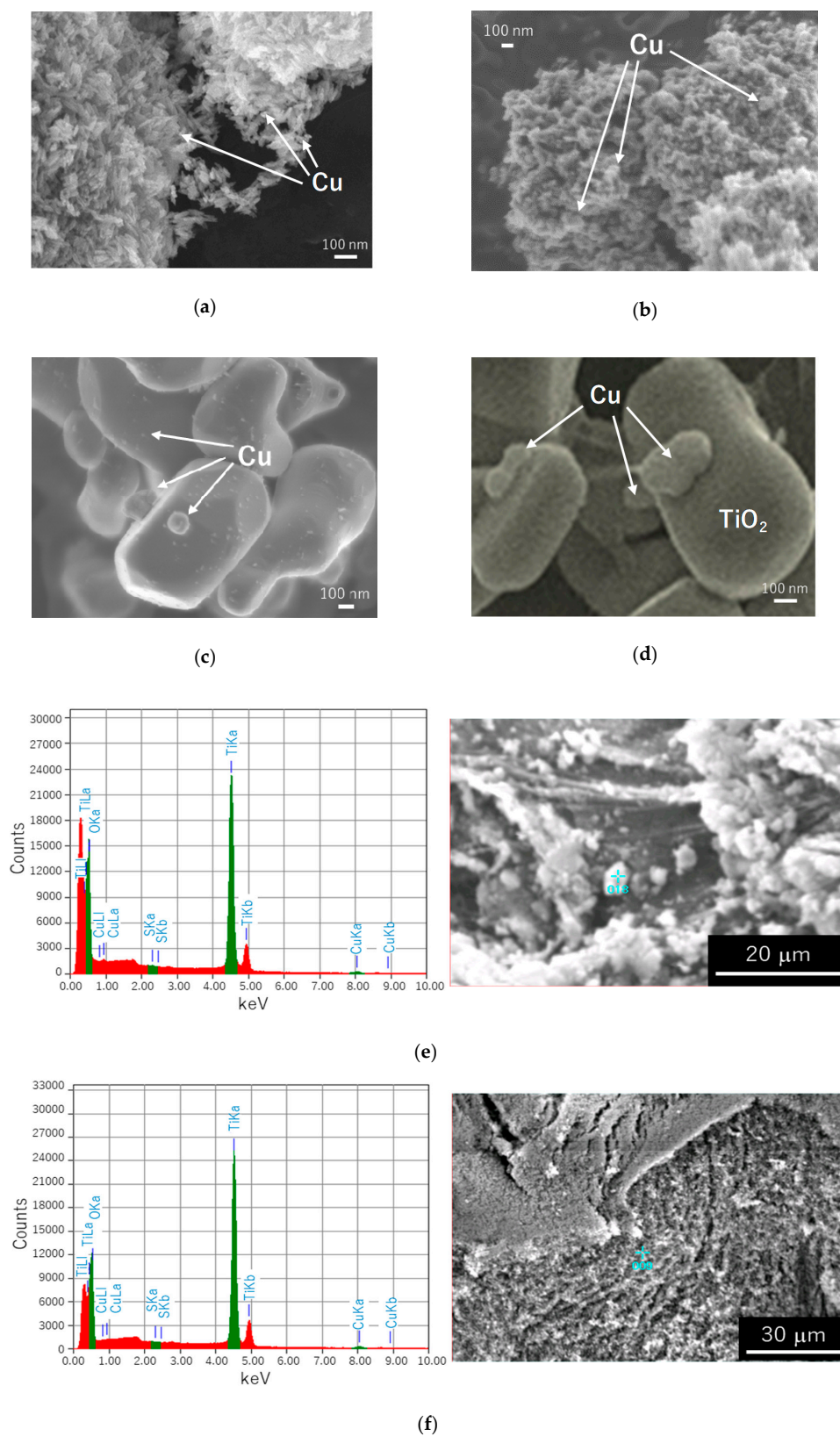


**Figure 4.** (a–d) Scanning electron microscopy (SEM) images of: (a) CuTIO-6m-1h, (b) CuTIO-6m-5h, (c) CuTIO-5m-1h and (d) CuTIO-5m-5h. (e,f) Energy-dispersive X-ray spectroscopy (EDS) and corresponding SEM images of (e) CuST-01m-5h and (f) CuST-41m-5h.

### 2.5. X-Ray Photoelectron Spectroscopy

For detailed analysis of surface composition of samples, including copper forms, XPS analysis has been performed, and summarized data are shown in Table 3. The oxygen to titanium ratio in all samples has exceeded that in chemical formula (2.0 for  $\text{TiO}_2$ ), as typical for titania samples due to adsorbed water and carbon dioxide. Moreover, the content of reduced form of titanium ( $\text{Ti}^{3+}$ ) has increased after copper deposition, as a result of reductive conditions during copper photodeposition, i.e., from 0.5% and 1.4% (bare titania) to 3.3–4.9% and 3.0–3.4% for P25 and TIO-5, respectively. Copper has been detected in all analyzed samples, and its content (Cu:Ti) exceeds that used for sample preparation (2 wt%, i.e., 0.025 of Cu(at):Ti(at)), which is reasonable considering that the surface of titania must be enriched with copper. Moreover, it has been confirmed that prolonged irradiation results in more efficient deposition of copper on titania (m-1h vs. m-5h). The Cu  $3p_{3/2}$  peak could be divided to at least four oxidation forms, i.e., zero-valent copper,  $\text{Cu}_2\text{O}$ ,  $\text{CuO}$  and  $\text{Cu}(\text{OH})_2$  with binding energies of about 930, 932, 933 and 934 eV, respectively. For P25 samples, XPS results agree well with DRS data (Figure 2c), i.e., the higher content of zero-valent copper for samples prepared in methanol (corresponding to more intense absorption at LSPR range) than prepared in water, and high content of cuprous oxide in CuP25m-1h sample (clear absorption peak at about 470 nm). Interestingly, samples prepared in water (both P25 and TIO-5) contain the smallest content of zero-valent copper, suggesting that reduction of copper during water oxidation might not been completed (Equation 4). Summarizing, XPS data confirm the co-existence of different forms of copper in the samples prepared by photodeposition methods.

**Table 3.** Surface composition of samples determined by X-ray photoelectron spectroscopy (XPS) analysis.

Samples	Content (at %)				Cu/Ti	Ti $2p_{3/2}$ (%)		Cu $2p_{3/2}$ (%)				
	C 1s	O 1s	Ti $2p_{3/2}$	Cu $2p_{3/2}$		Ti <sup>3+</sup>	Ti <sup>4+</sup>	Cu	Cu <sub>2</sub> O	CuO	Cu(OH) <sub>2</sub>	
P25	bare	47.1	39.7	13.2	-	-	0.5	99.5	-	-	-	-
	m-1h	39.9	39.8	18.9	1.4	0.075	3.6	96.4	7.9	79.2	12.4	0.5
	w-1h	49.2	35.2	14.7	0.9	0.059	3.3	96.7	1.5	28.3	69.6	0.6
	m-5h	47.8	36.1	14.7	1.5	0.099	4.9	95.1	18.8	70.0	8.3	2.9
TIO-5	bare	47.0	40.1	12.9	-	-	1.4	98.6	-	-	-	-
	m-1h	49.7	34.8	13.3	3.0	0.180	3.4	96.6	8.5	25.6	59.4	6.5
	w-1h	54.3	32.4	11.3	2.0	0.220	3.0	97.0	0.3	71.9	3.4	24.4
	m-5h	49.8	34.6	13.1	2.6	0.195	3.0	97.0	8.1	15.9	43.5	32.5

### 2.6. Photocatalytic Activity

The oxidative decomposition of acetic acid to  $\text{CO}_2$  and  $\text{H}_2\text{O}$  on the surface of irradiated titania is a common reaction used for photocatalytic activity testing [44]. Although bare  $\text{TiO}_2$  is also able to decompose acetic acid (black bars in Figure 5a), the reaction rate is limited due to charge carriers' recombination. Accordingly, noble metals in both zero-valent and oxide forms have been used to hinder this recombination via scavenging of photogenerated electrons and heterojunction between two oxides (p-n junction or/and Z-scheme mechanism), respectively [81,82,87–90]. Indeed, modification with copper enhances the photocatalytic activity, especially for anatase samples, by 2–3 times, as shown in Figure 5a. Interestingly, shorter irradiation during copper photodeposition results in better photocatalytic performance (red vs. green bars), due to the unwanted aggregation of copper deposits during prolonged irradiation, and thus worse distribution of copper on titania (fewer active sites for reaction).

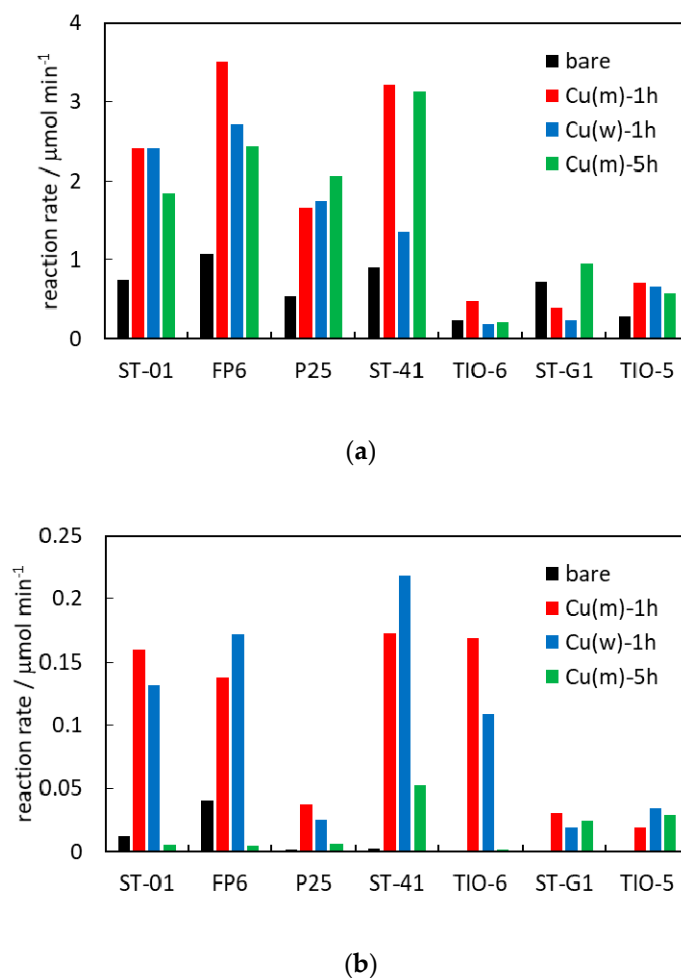


**Figure 5.** Comparison of photocatalytic efficiency for acetic acid decomposition under: (a) ultraviolet/visible (UV/vis) and (b) vis irradiation.

It should be pointed out that mainly oxidized forms of copper have been detected in present samples, and thus the activity enhancement by type II heterojunction or Z-scheme mechanism for  $\text{Cu}_x\text{O}$  and  $\text{TiO}_2$  might be considered as predominant mechanism. Interestingly, the  $\text{Cu}_2\text{O}/\text{TiO}_2$  photocatalysts, prepared by the grinding of commercial  $\text{Cu}_2\text{O}$  and different titania samples, have shown similar activity enhancement, i.e., 4–5 times for samples containing of anatase and only slight enhancement for those with rutile [87]. It has been proposed that due to more negative potential of the conduction band (CB) of rutile than anatase [79], type II heterojunction for rutile/ $\text{Cu}_2\text{O}$  and Z-scheme mechanism for anatase/ $\text{Cu}_2\text{O}$  are most probable [87]. The latter is preferential, resulting in the generation of charges with stronger redox potential (electrons in CB of  $\text{Cu}_2\text{O}$  and positive holes in VB of  $\text{TiO}_2$ ). It has been proved that photocatalytic activity for the oxidation reactions depends directly on the oxidation potential of photogenerated holes, and anatase is a stronger oxidant than rutile, due to the more positive position of the VB [79]. Accordingly, lower activities of rutile might be simply explained by less positive potential of its VB. In this regard, it has been considered that the more negative potential of CB of rutile might cause a type II heterojunction with not so good redox properties (electrons in CB of titania and holes in VB of cuprous oxide), and thus not so high improvement of photocatalytic activity. It should be pointed that although the content of zero-valent copper is low, the function of copper as an electron scavenger should not be omitted since it is known that even a very low content of noble metals might cause significant enhancement of activity, e.g., 0.05 wt% of Au [90]. Therefore, participation of all forms of copper might be responsible for activity enhancement, e.g., by cascade mechanism or Z-scheme with co-electron scavenging by zero-valent copper, etc.

The photocatalytic activity under vis ( $\lambda > 450$  nm) irradiation has also been evaluated, and obtained data are shown in Figure 5b. Although acetic acid decomposition under vis irradiation is much slower than that under UV (by about one order), the vis-activity of copper-modified titania has been proven. In contrast to UV activity, prolonged irradiation during samples' preparation (green bars) has resulted in a significant decrease in activity, especially for fine titania samples. Accordingly, it is proposed that aggregation of copper NPs is highly detrimental for fine titania samples. It should be reminded that titania absorbs only UV light, whereas under vis irradiation, only copper species (except FP6 titania with some defects) might absorb photons, and thus larger particles (aggregates) mean less species absorbing photons and lower interface between titania and copper, and thus lower probability for efficient charge carriers' transfer. Although, various mechanisms of oxidative decomposition of organic compounds on copper-modified titania under vis irradiation have already been proposed, including (i) plasmonic excitation (for zero-valent copper) [82], (ii) type II heterojunction with an electron transfer from the CB of copper oxides ( $\text{Cu}_2\text{O}/\text{CuO}$ ) to CB of titania [87], and (iii) interfacial charge transfer with excitation of electrons from VB of titania into CB of  $\text{Cu}_x\text{O}$  [86], it is highly probable that those mechanisms might proceed simultaneously, depending on the photocatalyst's properties, i.e., especially the form of copper and its content.

It should be pointed out that the activity under vis irradiation for copper-modified titania differs significantly from that for gold-modified titania samples, where the highest activity has been obtained for large rutile samples (the same titania samples as used in this study) with aggregated gold deposits [44,91,92]. Additionally, other studies have also confirmed that for plasmonic photocatalysis, an increase in the polydispersity of noble metals result in higher activity as a result of efficient light harvesting (broad LSPR peak and strong field enhancement) [93,94]. Therefore, it might be postulated that here the vis activity of copper-modified titania is mainly caused by copper oxides, which correlates well with the activity of  $\text{Cu}_2\text{O}/\text{TiO}_2$  photocatalysts (except ST-41 samples), prepared by grinding, i.e.,  $\text{Cu}_2\text{O}/\text{TIO-6} > \text{Cu}_2\text{O}/\text{ST-01} > \text{Cu}_2\text{O}/\text{P25} > \text{Cu}_2\text{O}/\text{ST-41} > \text{Cu}_2\text{O}/\text{large rutile}$  [87]. The highest activity of copper-modified large anatase (ST-41) samples, especially that prepared in water, should be caused by the presence of CuO (Figure 2d), which has recently been reported as highly active under vis irradiation [95]. Moreover, only TIO-6 samples exhibit high activity among the rutile group. Therefore, in the case of acetic acid decomposition under vis irradiation, the presence of CuO (as confirmed in DRS spectra) is beneficial for the activity. Accordingly, it might be concluded that for vis activity the copper oxides might be more active than plasmonic photocatalysts. However, it should be pointed out that in the case of easily oxidizable metal (Cu), only slight content of zero-valent copper has been kept in the samples (after their surface oxidation in air), and thus the preparation of samples with stabilized copper should be performed, which is now under progress (e.g.,  $\text{Cu}(\text{core})/\text{TiO}_2(\text{shell})$  photocatalysts), to conclude which forms of copper in Cu-modified  $\text{TiO}_2$  are the most recommended.

### 2.7. Antibacterial Activity

The bactericidal activities against Gram-negative *Escherchia coli* of copper-modified titania photocatalysts have been evaluated under vis irradiation and in the dark (Figure 6). Although bare anatase samples do not exhibit high activity, bare rutile samples are shown to be active (Figure 6e,f), which might be explained by the narrower bandgap of rutile, and thus slight content of ETs inside bandgap (self-doped titania; Table 1) resulting in slight vis response. Recently, high antibacterial activity of samples containing rutile against various bacteria (e.g., *E. coli*, *Bacillus subtilis*, and *Staphylococcus aureus*) under fluorescent irradiation has been confirmed by Werapun and Pechwang [96]. Moreover, it has been reported that rutile particles (200 nm) induce hydrogen peroxide formation and oxidative DNA damage for human bronchial epithelial cells in the dark condition, whereas anatase particles (200 nm) do not [97]. Similarly, Vargas and Rodríguez-Páez concluded that rutile NPs possess higher antibacterial efficiency than anatase NPs in the dark [98].

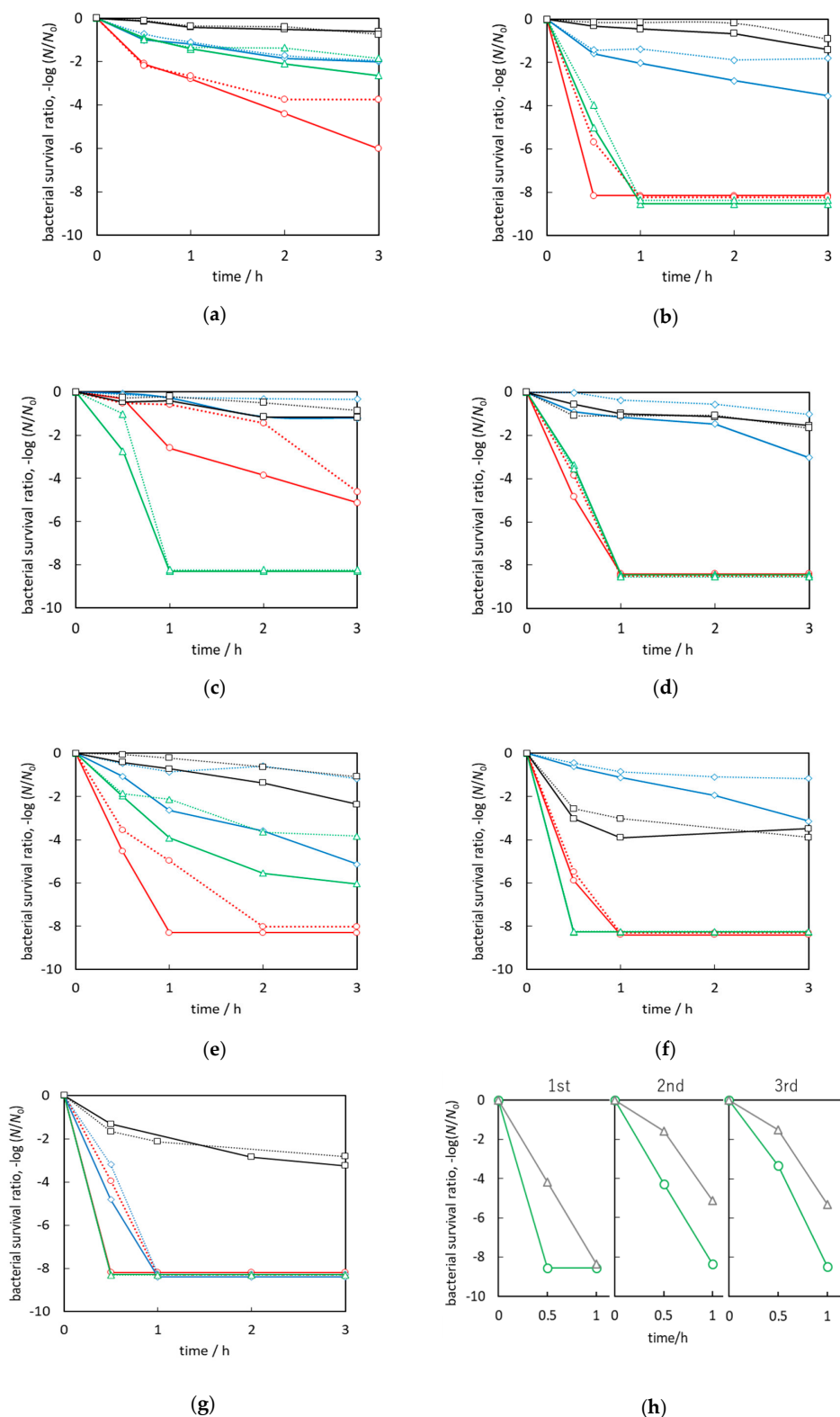


**Figure 6.** Bactericidal activities of bare and copper modified titania: (a) ST-01, (b) FP6, (c) P25, (d) ST-41, (e) TIO-6, (f) ST-G1 and (g) TIO-5 (black: bare, red: m-1h, blue: w-1h, green: m-5h) under visible light (solid line) and in the dark (dashed line); (h) the activity of CuTIO-5m-1h photocatalyst during three successive experiments under vis irradiation (green) and in the dark (grey).

It has been found that the properties of photocatalysts influence significantly antibacterial activity. For example, photocatalysts with fine particles (CuST-01 and CuTIO-6) show relatively

lower activity than respective titania (anatase or rutile) but with larger particles, e.g., CuST-41 and CuTIO-5, respectively. The bactericidal activity of the CuP25m-5h sample is much higher than other P25-containing samples, possibly due to higher copper content (Cu/Ti ratio) on its surface (Table 3). Moreover, the comparison between large anatase and rutile indicates that rutile samples (CuST-G1 and CuTIO-5) exhibit higher activity than the anatase one (CuST-41). Across all samples, the samples formed in methanol possess much higher bactericidal activity than those in water, possible due to much larger content of zero-valent copper (Table 3). However, interestingly, CuTIO-5w-1h sample shows also high activity, comparable to those by samples prepared in methanol (CuTIO-5m-1h and CuTIO-5m-5h), probably due to the presence of Cu<sub>2</sub>O (Figure 3g), known as the most active form of copper against bacteria. On the other hand, the light-induced activity is mainly observed in m-1h samples, but not in m-5h samples, probably due to aggregation of copper NPs, and a decrease in the interface between copper and bacteria. Importantly, high difference between the activities during decomposition of acetic acid and bacteria have been noticed, since the bactericidal activity is highly dependent on the oxidation state of copper, e.g., the optimal ratio proposed for Cu<sub>x</sub>O clusters (Cu<sub>2</sub>O/CuO = 1.3) is critical for the antimicrobial activity [72].

Interestingly, the samples prepared by grinding Cu<sub>2</sub>O with titania show much higher activity enhancement during vis irradiation (even 4–7 orders in magnitude higher activity than that in the dark) [87], whereas the samples, prepared in this study by photodeposition of copper, exhibit only at most two orders of magnitude higher vis-activity than that in the dark (e.g., CuFP6m-1h during first 30 min; red lines in Figure 6b). Accordingly, it might be concluded that co-existence of other copper species, i.e., zero-valent copper and CuO, result in high dark activity of these samples.

Moreover, although the bactericidal activity of Cu<sub>2</sub>O/ST-01 (ground sample) has been much higher than CuST-01 (prepared here), other titania samples (P25, ST-41 and TIO-6) exhibit similar activity under vis irradiation (depending on the synthesis conditions) [87], and thus the bactericidal activity of Cu-modified titania might be attributed not only to the initial content of Cu<sub>2</sub>O (Table 2), but also the charge-transfer during the irradiation, including plasmonic photocatalysis [99].

The possible mechanism of antimicrobial action of copper-modified titania under vis irradiation has been explained by Wang et al. [100], where generated reactive oxygen species, such as O<sub>2</sub><sup>•−</sup>, •OH or H<sub>2</sub>O<sub>2</sub>, have been proposed to cause an oxidative stress and cell disruption. Additionally, part of the copper might be released from the photocatalyst surface, and adsorb on the bacteria surface (or cross bacterial membrane). However, the toxic mechanism of copper has not been clarified yet. It has been proposed that the excess copper ions might interact with functional group of enzymes, required for defense against oxidative damage or other copper/zinc proteins (Cu ions compete with zinc for important binding sites). The generation of reactive hydroxyl radicals in a Fenton-type reaction has also been proposed as one of the possible mechanisms of bacteria inactivation [101].

The stability of the photocatalyst (CuTIO-5m-1h) has been investigated during three successive experiments under vis irradiation and in the dark, and obtained results are shown in Figure 6h. The activity decreases after the first experiment, especially in the dark, but almost the same performance has been observed during the second and third experiments. Accordingly, it might be concluded that even when initial activity has been decreased (probably due to the change in the surface composition of copper: Cu/Cu<sub>2</sub>O/CuO as a result of direct redox reaction with bacteria), the photocatalyst might be efficiently reused, maintaining a high performance, i.e., complete bacteria inactivation during 1 h vis irradiation.

Summing up, copper-modified titania photocatalysts have proven to be a promising candidate for preparation of antibacterial materials or active coatings under vis irradiation. In comparison with other Cu-modified titania prepared by different methods (e.g., sol-gel [102] and impregnation [72] method), CuTiO<sub>2</sub> samples inactivated bacteria much faster. Moreover, the dark activity of the samples was significant, indicating the possibility of efficient use in an indoor environment. Nevertheless, antibacterial activity against only one type of model bacteria is limited in scope, and thus more studies against different bacteria, especially antibiotic resistant (ABR) ones should be carried out.

## 2.8. Antifungal Activity

The filamentous or mould fungi are eukaryotic microorganisms that have a more complex morphology of cells and cell-walls structures than prokaryotic bacteria. Due to this difference, fungi are generally more resistant to the antimicrobial agents, drugs [103] and photocatalytic process [104]. That is caused by high chitin content (around 15% of cell wall dry mass) in cell walls, which protects fungi against mechanistic and oxidative damage. A relatively thick layer of polysaccharide (chitin) cover is also resistant to oxidative stress due to a glucan layer, mainly composed of  $\beta$ -1,3-glucan. Extracellular layer of fungal cell wall is formed by glycoproteins which are very sensitive to oxidative damage (around 15% of cell wall dry mass). Pigments, such as dark-brown melanin (in a fungal cell wall) protect them against some environmental factors e.g., UV radiation and ionizing radiation [105]. The importance of the cell wall for fungal cells and their spore survival during the photocatalytic process has been proven by Kühn et al. [106]. Additionally, in our previous study, it has been shown that antimicrobial activity depends on the type of noble metal, e.g., silver-modified titania activated under vis irradiation shows the highest bactericidal activity, whereas gold-modified titania are the most active against fungi [107]. Therefore, since the bactericidal materials do not necessarily inhibit the fungal growth, the fungistatic performance of these Cu-modified titania is now described. The recent study has shown that copper is micronutrient for fungal growth and proliferation, but might also generate toxicity and even cell-death [108].

The antifungal activity of anatase samples (CuST-01m-1h, CuFP6m-1h and CuST-41m-1h) was evaluated against *Aspergillus niger*, under both dark and vis irradiation conditions, by the agar disc diffusion method (Figure 7). No inhibition zones were observed and fungi were overgrown over all the plate's surface, excluding only the paper discs, Figure 7b–d. The only exception was for the control sample (0.9% NaCl solution) for which mold covered also paper discs (Figure 7a). In other words, Cu-modified titania in concentration of 1 g/L suppressed the fungal growth on the surface without obvious differences between vis and dark conditions. Therefore, slight fungistatic activity of Cu-modified titania was not caused by photocatalytic activity but rather by the antifungal properties of copper. Moreover, no clear differences among copper-modified titania samples could be noticed. In addition, as reported previously [107], the lack of inhibition zones (around paper discs) indicate the stability of metallic deposits on the titania surface (no leakage).

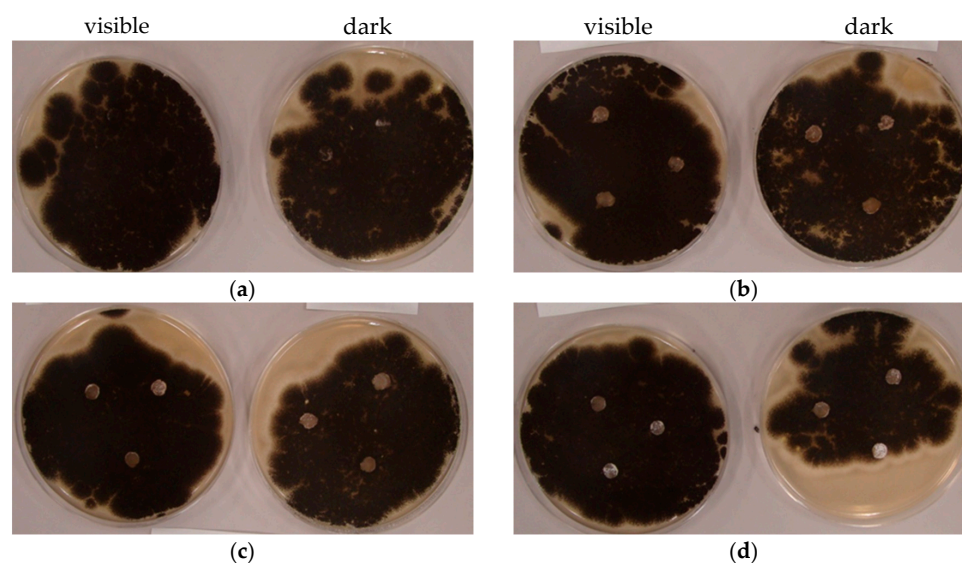


**Figure 7.** The photographs of *Aspergillus niger* colony on Malt Extract Agar (MEA) plates: (a) 0.9% NaCl (control), (b) CuST-01m-1h, (c) CuFP6m-1h, (d) CuST-41m-1h, incubated under vis (left) and in the dark (right).

Chen et al. showed that growth of *A. niger* on wood surfaces coated with TiO<sub>2</sub> film was completely inhibited after 20 days under UV light of 365 nm wavelength [109]. Despite such a long time of exposure, fungal spores have remained viable and their re-growth has been observed when irradiation was stopped. Taking into account the results obtained in this study, it has been concluded that vis irradiation is insufficient to activate copper-modified TiO<sub>2</sub> during the first period of fungal growth. A previous study, upon nitrogen-doped TiO<sub>2</sub> activated by indoor light, demonstrated a significant effect in the first 48 h of incubation, when the germination phase of spores takes place [110], and this is followed by the elongation of white (i.e., melanin-free) hyphae [111]. Although significant differences in the initiation of melanin production exist among filamentous fungi, for *Aspergillus* species, this is characterized by darkening of the hyphae and formation of mature conidiophores. Melanin is a powerful free-radical scavenger, acting as a sponge for intracellular free radicals generated when environmental factors place the cell under oxidative stress [112]. Thus, there seems little rationale for prolongation of irradiation during these vis irradiation tests. The real challenge is to find a photocatalyst, which is suitable to stop production of melanin within 24 h by as many fungal species as achievable. For further analysis, the other method should be also applied, for example sporulation tests (next paragraph). The mechanism deserves further investigation, because the effects might help to optimize the methodology for antifungal susceptibility testing and developing photocatalytic self-cleaning building materials or coatings, air cleaners, and filters used to remove the microorganism from indoors aerosol and surfaces, especially where UV-A exposure is not possible (under visible light).

The fungistatic activity against *A. niger* has also been investigated by the spore-counting method under fluorescence light and in the dark (Figure 8). The CuFP6m-1h sample significantly suppresses the generation of spores under both conditions, but the mycelium has been still observed (Figure 8b), indicating that only sporulation is inhibited. A pristine FP6 sample also exhibits slight inhibition of sporulation, since fluorescence light contains a small portion of UV. It should be pointed out that the number of spores in the dark for both samples is smaller than that under irradiation, possibly due to the stimulation of fungal growth and sporulation by light [110,113–115]. Therefore, it is proposed that fungal growth might exceed the photocatalytic fungistatic effect [88]. Moreover, some proteins and sugars on fungal cells can be easily adsorbed on titania (independent on the irradiation) [116–119].

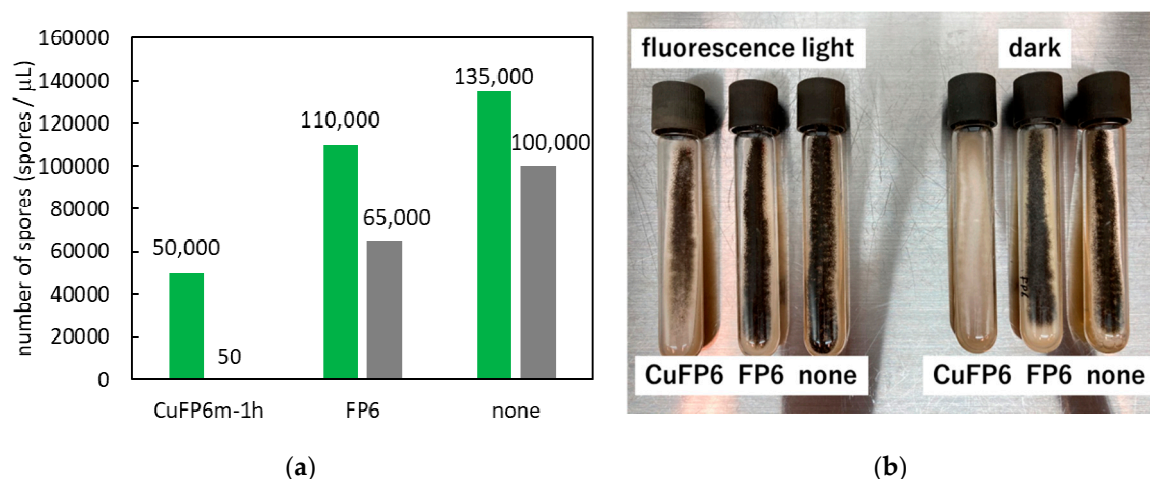


**Figure 8.** Sporulation tests: (a) number of spores after 3-day growth of *A. niger* under fluorescence light (green bars) and in the dark (grey bars); and (b) representative photographs of slants for CuFP6m-1h, FP6 and in the absence of photocatalyst.

Additionally, the presence of melanin in the spore protects the fungal cells against ROS [112] and light. The increased inhibition of sporulation and melanization observed for CuFP6m-1h can be explained by the possibility of increased copper uptake through the action of one of the family of methionine-rich copper transport proteins. These transmembrane proteins are expected to be mostly

similar to those already characterized for *A. fumigatus* and *A. nidulans* [108]. Moreover, as mentioned above, mycelium growth is not inhibited and this is in accordance with a previous study which showed *A. niger* to be an efficient organism for bioremediation of copper-rich waste streams [120], where removal of copper was accompanied by a growth in mycelium but without growth of conidia or spores.

### 3. Materials and Methods

#### 3.1. Preparation of Cu-Modified Titania

Seven commercial titania samples, i.e., ST-01 (Ishihara Shangyo Kaisha, Ltd., Osaka, Japan), FP6 (Showa Denko Ceramics Co. Ltd., Tokyo, Japan), P25 (AEROXIDE® TiO<sub>2</sub> P25 produced by Nippon Aerosil Co., Ltd., Tokyo, Japan), ST-41 (Ishihara Shangyo Kaisha, Ltd., Osaka, Japan), TIO-6 (Catalysis Society of Japan, Tokyo, Japan), ST-G1 (Showa Denko Ceramics Co. Ltd., Tokyo, Japan) and TIO-5 (Catalysis Society of Japan, Tokyo, Japan), were used without pretreatment for the surface modification with copper (Table 1). We mixed 600 mg of TiO<sub>2</sub> with 0.94 mL of 0.2 M CuSO<sub>4</sub>·5H<sub>2</sub>O (99.9%, FUJIFILM Wako Pure Chemical Corporation, Osaka, Japan) aqueous solution in a 50 mL Pyrex-glass tube containing of 26.3 mL of 50 vol% methanol-water (Milli-Q) solution. Samples were also prepared in the absence of alcohol, i.e., in 26.3 mL of Milli-Q water. The suspension was deaerated with argon pre-bubbling, and the tube was tightly closed with a rubber septum and wrapped in parafilm. The samples were irradiated under ultraviolet light, using home-built high-pressure Hg lamp ( $\lambda > 220$  nm, output power of 400 W, light intensity of about 20 mW cm<sup>-2</sup>) in a thermostatic water bath at 25 °C under continuous stirring (500 rpm) for 1 or 5 h. Before and during irradiation, 0.2 mL of the gas sample was taken from the tube with a syringe and the amount of evolved H<sub>2</sub> or O<sub>2</sub> (in the case of methanol/water and water, respectively) was detected by gas chromatography with a thermal conductivity detector (GC-TCD; GC-8A, SHIMADZU CORPORATION, Kyoto, Japan). After irradiation, the samples were collected by centrifugation (3000 rpm), washed twice by resuspending in the methanol (followed by centrifugation), then washed twice by resuspending in water (followed by centrifugation), and finally dried overnight at 120 °C. Then, samples were ground in an agate mortar. The code names of samples indicate the titania type (ST-01, FP6, P25, ST-41, TIO-6, ST-G1 and TIO-5), environment (water (w) or methanol/water (m)) and duration (1 h or 5 h) of irradiation, e.g., the CuST-01m-1h sample was prepared by deposition of copper on ST-01 titania in a methanol/water solution during 1 h irradiation.

#### 3.2. Characterization

Photoabsorption properties of samples were analyzed by diffuse reflectance spectroscopy (DRS; JASCO V-670 equipped with a PIN-757 integrating sphere, JASCO, LTD., Pfungstadt, Germany). Barium sulfate was used as a reference for DRS analysis. For the characterization of crystal structure, X-ray powder diffraction (XRD; Rigaku intelligent XRD SmartLab with a Cu target, Rigaku, LTD., Tokyo, Japan) was operated (accelerating voltage: 40kV, emission current: 30 mA). The samples were investigated between 10° and 90° at 1°/min scan speed and scan step of 0.008°. The crystal structures were analyzed with Rigaku PDXL software (Version 2.6.1.2, Rigaku, LTD., Tokyo, Japan, 2007–2015). Crystallite sizes of anatase, rutile, Cu and Cu<sub>2</sub>O were estimated by the Scherrer equation, using the Joint Committee on Powder Diffraction Standards (JCPDS) card numbers of 5757, 7818, 31057, 8728, respectively. The surface properties of samples and the oxidation states of elements were analyzed by X-ray photoelectron spectroscopy (XPS; JPC-9010MC, JEOL, Tokyo, Japan). At first, samples were attached to carbon tape on a sample holder and dried under a vacuum. The Mg X-ray source, 10 V accelerating voltage and 10 mA emission current under high vacuum were set as operation conditions. The binding energies were examined between 1000 eV and 0 eV and for specific ranges depending on the binding energies of elements. The data were evaluated using JEOL SpecSurf Software (Version 1.7.3.9, JEOL, Tokyo, Japan, 2000). All graphs were charge-corrected with a

carbon 1s peak to 284.7 eV. The morphology of the samples was analyzed by field emission-scanning electron microscopy (FE-SEM; JSM-7400F, JEOL, Tokyo, Japan) under a high vacuum. The samples were spread on carbon paste and dried under a vacuum overnight. Images were acquired in a wide range of magnifications in secondary electron imaging mode (SEI). Samples were also analyzed by energy-dispersive X-ray spectroscopy (EDS, JSM-6360 LA Analytical SEM, JEOL, Tokyo, Japan) under high vacuum to investigate the chemical composition of copper-modified titania.

### 3.3. Photocatalytic Activity Tests

The photocatalytic activity of samples was investigated for oxidative decomposition of acetic acid under UV/vis and vis irradiation. Fifty milligrams of sample were dispersed in 5 mL of 5 vol% acetic acid in a Pyrex-glass test tube. The suspension was irradiated with a home-made Hg lamp ( $\lambda > 220$  nm) or Xe lamp (output power 450 W, light intensity about  $20 \text{ mW cm}^{-2}$ ,  $\lambda > 450$  nm; water IR filter, cold mirror and cut-off filter Y48) in a thermostat water bath at  $25^\circ\text{C}$  under continuous stirring. The generated carbon dioxide was measured by GC-TCD or gas chromatography with flame ionization detector (GC-FID; SHIMADZU CORPORATION, Kyoto, Japan), respectively.

### 3.4. Bactericidal Tests

The bactericidal activity was evaluated under vis irradiation ( $\lambda > 450$  nm) using *Escherichia coli* K12 (ATCC 29425, ATCC, Manassas, VA, USA), as described elsewhere [107]. In brief, a 50 mg of sample was suspended in 5 mL of *E. coli* suspension (about  $1\sim 5 \times 10^8$  cells/mL) in a Pyrex-glass test tube. The suspension was irradiated with Xe lamp ( $\lambda > 450$  nm) or kept in the dark (control experiment) under continuous stirring at  $25^\circ\text{C}$ . During irradiation (i.e., at 0.5, 1, 2 and 3 h), a portion of suspension was withdrawn, diluted and inoculated on the Plate Count Agar (Becton, Dickinson and Company, Franklin Lakes, NJ, USA) medium. Agar plates were incubated at  $37^\circ\text{C}$  overnight, and then the bacterial colonies were counted to calculate the colony-forming unit/mL (CFU/mL). The bacterial survival ratio was computed, and presented as  $-\log(N_t/N_0)$ , where  $N_0$  is the initial number of bacteria, and  $N_t$  is the number of bacteria after time  $t$ . For the reusability test, the titania sample (CuTiO-5m-1h) was collected by leaving it to stand, washing it with sterile Milli-Q water, and drying it at  $120^\circ\text{C}$ . Then, the same experiment was repeated twice.

### 3.5. Antifungal Tests

#### 3.5.1. Disc Diffusion Test

The antifungal tests were performed with mould fungus, *Aspergillus niger*, isolated from damp basement air (Zachodniopomorski Uniwersytet Technologiczny (ZUT) collection, Szczecin, Poland). The antifungal activity of the photocatalysts was tested using the disc diffusion method [121]. Culture plates were prepared with 20 mL of Malt Extract Agar (MEA; Merck, Darmstadt, Germany). Sterilized culture media were poured into Petri dishes and, after solidification of the medium, 0.25 mL of fungal suspension was spread on the plate using a spreader. The concentration of microorganisms was about  $10^6$  CFU/mL. The sterile paper discs (Whatman No.1, diameter 5 mm) impregnated with 10  $\mu\text{L}$ /disc photocatalyst suspension in concentration of 1 g/L (10  $\mu\text{L}$ /disc) were placed at different locations on the culture plates. The control discs were impregnated with saline solution (0.9% NaCl). The plates were incubated both in the dark and under indoor fluorescence light (intensity of about 120 lx) for 72 h. The temperature was maintained at about  $25^\circ\text{C}$ .

#### 3.5.2. Spore-Counting Test

CuFP6m-1h and bare FP6 samples (10 g/L) in MEA were autoclaved and the agar slants were prepared. Spores of *A. niger* (1000 cells/ $\mu\text{L}$ ) were suspended in 8.5 g/L NaCl aqueous solution, 20  $\mu\text{L}$  of spore suspension was inoculated on the agar slants and irradiated with fluorescence light (intensity of

about 120 lx) or kept in the dark for 3 days (about 23 °C). Generated spores were collected with 0.05% Triton X-100 in NaCl solution by vortex mixing and counted under an optical microscope.

#### 4. Conclusions

Surface modification of titania with copper results in the preparation of highly active photocatalysts under both UV and vis irradiation, due to the inhibition of charge-carrier recombination and vis absorption by copper species (Cu, Cu<sub>2</sub>O, CuO and Cu<sub>x</sub>O), respectively. The conditions during samples' preparation, i.e., time and medium (reaction system) and titania properties (size and crystalline composition) have governed the properties of formed Cu NPs, such as size, composition and oxidation state, and thus resultant activities. Since copper is easily oxidizable, it is thought that even though zero-valent Cu NPs are formed during methanol dehydrogenation, these NPs are easily oxidized in air, and thus co-mixed copper deposits have been obtained in all samples. The aggregation of copper during prolonged deposition results in the formation of copper deposits with a larger content of zero-valent copper (as a core). In the case of copper photodeposition during water oxidation, the least content of zero-valent copper was obtained, probably due to insufficient copper cations' reduction. It should be pointed out that even though the same method of copper deposition was used, as well as the same copper source and its content, a difference in titania kind resulted in preparation of samples with significantly different properties, and thus overall activities, e.g., one order for acetic acid decomposition and few orders for bacteria inactivation.

The modification of titania with copper causes a significant increase in the activity under UV irradiation, especially for anatase samples, suggesting the enhancement according to a Z-scheme mechanism between two types of semiconductor, i.e., copper oxides and anatase. Copper-modified samples have also been active under vis irradiation, but those activities do not correlate with the content of zero-valent copper, and thus it is thought that the p-n junction between two oxides (with electron transfer from CB of Cu<sub>2</sub>O to CB of TiO<sub>2</sub>) rather than plasmonic photocatalysis is the main driving force of vis response. Moreover, modified samples exhibit antimicrobial activity under both vis irradiation and in the dark. Although vis-irradiation has increased activity only slightly (predominant activity in the dark resulting from intrinsic properties of Cu, mainly Cu<sub>2</sub>O), the overall antibacterial effect is very high, causing complete inactivation of bacteria within 0.5–1 h for rutile-containing samples. Unfortunately, the mixed-oxidation state of copper in all samples makes it difficult to establish the key-factor properties for high photocatalytic activity. Despite that, it is believed that copper-modified titania are promising photocatalysts for broad environmental application because of low price, availability and high activity for decomposition of both organic compounds and microorganisms.

**Author Contributions:** Conceptualization, E.K., writing—original draft preparation, M.E.-K. and B.K., writing-revision and editing, M.E.-K., K.W., Z.W., A.M.-S., B.O. and E.K., sample preparation, B.K. and K.W., sample characterization and photoactivity tests, M.E.-K., K.W. and B.K., microbiological tests, M.E.-K., B.K. and A.M.-S., data analysis, M.E.-K., K.W., Z.W., A.M.-S. and E.K., supervision, E.K., funding acquisition, E.K. and B.O. All authors have read and agreed to the published version of the manuscript.

**Funding:** This work was financially supported by a Grand Challenges Explorations Grant (GCE RB, OPP1060234) from Bill and Melinda Gates Foundation, and “Yugo-Sohatsu Kenkyu” for an Integrated Research Consortium on Chemical Sciences (IRCCS) project from the Ministry of Education and Culture, Sport, Science and Technology-Japan (MEXT). The APC was funded by Z.W., A.M.-S. and E.K.

**Conflicts of Interest:** The authors declare no conflict of interest.

#### References

1. Hoffmann, M.R.; Martin, S.T.; Choi, W.; Bahnemann, D.W. Environmental applications of photocatalysis. *Chem. Rev.* **1995**, *95*, 69–96. [[CrossRef](#)]
2. Wang, Y.; Huang, Y.; Ho, W.; Zhang, L.; Zou, Z.; Lee, S. Biomolecule-controlled hydrothermal synthesis of C-N-S-tridoped TiO<sub>2</sub> nanocrystalline photocatalysts for NO removal under simulated solar light irradiation. *J. Hazard. Mater.* **2009**, *169*, 77–87. [[CrossRef](#)] [[PubMed](#)]

3. Su, C.; Tseng, C.M.; Chen, L.F.; You, B.H.; Hsu, B.C.; Chen, S.S. Sol-hydrothermal preparation and photocatalysis of titanium dioxide. *Thin Solid Films* **2006**, *498*, 259–265. [[CrossRef](#)]
4. Martin, S.T.; Lee, A.T.; Hoffmann, M.R. Chemical mechanism of inorganic oxidants in the TiO<sub>2</sub>/UV process: Increased rates of degradation of chlorinated hydrocarbons. *Environ. Sci. Technol.* **1995**, *29*, 2567–2573. [[CrossRef](#)]
5. Verbruggen, S.W. TiO<sub>2</sub> photocatalysis for the degradation of pollutants in gas phase: From morphological design to plasmonic enhancement. *J. Photochem. Photobiol. C Photochem. Rev.* **2015**, *24*, 64–82. [[CrossRef](#)]
6. Fujishima, A.; Honda, K. Electrochemical photolysis of water at a semiconductor electrode. *Nature* **1972**, *238*, 37–38. [[CrossRef](#)]
7. Fujishima, A.; Rao, T.N.; Tryk, D.A. Titanium dioxide photocatalysis. *J. Photochem. Photobiol. C Photochem. Rev.* **2000**, *1*, 1–21. [[CrossRef](#)]
8. Byrne, C.; Subramanian, G.; Pillai, S.C. Recent advances in photocatalysis for environmental applications. *J. Environ. Chem. Eng.* **2018**, *6*, 3531–3555. [[CrossRef](#)]
9. Ohtani, B.; Prieto-Mahaney, O.O.; Li, D.; Abe, R. What is degussa (Evonic) P25? Crystalline composition analysis, reconstruction from isolated pure particles and photocatalytic activity test. *J. Photochem. Photobiol. A Chem.* **2010**, *216*, 179–182. [[CrossRef](#)]
10. Crampton, A.S.; Cai, L.; Janvelyan, N.; Zheng, X.; Friend, C.M. Methanol photo-oxidation on rutile TiO<sub>2</sub> nanowires: Probing reaction pathways on complex materials. *J. Phys. Chem. C* **2017**, *121*, 9910–9919. [[CrossRef](#)]
11. Liu, Y.; Chen, L.; Hu, J.; Li, J.; Richards, R. TiO<sub>2</sub> nanoflakes modified with gold nanoparticles as photocatalysts with high activity and durability under near UV irradiation. *J. Phys. Chem. C* **2010**, *114*, 1641–1645. [[CrossRef](#)]
12. Anitha, V.C.; Hamnabard, N.; Banerjee, A.N.; Dillip, G.R.; Joo, S.W. Enhanced electrochemical performance of morphology-controlled titania-reduced graphene oxide nanostructures fabricated via a combined anodization-hydrothermal process. *RSC Adv.* **2016**, *6*, 12571–12583. [[CrossRef](#)]
13. Huang, X.; Meng, L.; Du, M.; Li, Y. TiO<sub>2</sub> nanorods: Hydrothermal fabrication and photocatalytic activities. *J. Mater. Sci. Mater. Electron.* **2016**, *27*, 7222–7226. [[CrossRef](#)]
14. Bian, Z.; Tachikawa, T.; Zhang, P.; Fujitsuka, M.; Majima, T. Au/TiO<sub>2</sub> superstructure-based plasmonic photocatalysts exhibiting efficient charge separation and unprecedented activity. *J. Am. Chem. Soc.* **2014**, *136*, 458–465. [[CrossRef](#)] [[PubMed](#)]
15. Abbas, W.A.; Ramadan, M.; Faid, A.Y.; Abdellah, A.M.; Ouf, A.; Moustafa, N.; Allam, N.K. Photoactive catalysts for effective water microbial purification: Morphology-activity relationship. *Environ. Nanotechnol. Monit. Manag.* **2018**, *10*, 87–93. [[CrossRef](#)]
16. Stafford, U.; Gray, K.A.; Kamat, P.V.; Varma, A. An in situ diffuse reflectance FTIR investigation of photocatalytic degradation of 4-chlorophenol on a TiO<sub>2</sub> powder surface. *Chem. Phys. Lett.* **1993**, *205*, 55–61. [[CrossRef](#)]
17. Smirnova, N.; Fesenko, T.; Zhukovsky, M.; Goworek, J.; Eremenko, A. Photodegradation of stearic acid adsorbed on superhydrophilic TiO<sub>2</sub> surface: In situ FT-IR and LDI study. *Nanoscale Res. Lett.* **2015**, *10*, 1–7. [[CrossRef](#)]
18. Mamaghani, A.H.; Haghghat, F.; Lee, C.S. Role of titanium dioxide (TiO<sub>2</sub>) structural design/morphology in photocatalytic air purification. *Appl. Catal. B Environ.* **2020**, *269*, 118735. [[CrossRef](#)]
19. Ghosh, M.; Lohrasbi, M.; Chuang, S.S.C.; Jana, S.C. Mesoporous titanium dioxide nanofibers with a significantly enhanced photocatalytic activity. *ChemCatChem* **2016**, *8*, 2525–2535. [[CrossRef](#)]
20. Al-Mamun, M.R.; Kader, S.; Islam, M.S.; Khan, M.Z.H. Photocatalytic activity improvement and application of UV-TiO<sub>2</sub> photocatalysis in textile wastewater treatment: A review. *J. Environ. Chem. Eng.* **2019**, *7*, 103248. [[CrossRef](#)]
21. Ohtani, B. Preparing articles on photocatalysis—Beyond the illusions, misconceptions, and speculation. *Chem. Lett.* **2008**, *37*, 217–229. [[CrossRef](#)]
22. Anpo, M.; Takeuchi, M. The design and development of highly reactive titanium oxide photocatalysts operating under visible light irradiation. *J. Catal.* **2003**, *216*, 505–516. [[CrossRef](#)]
23. Karvinen, S.; Hirva, P.; Pakkanen, T.A. Ab initio quantum chemical studies of cluster models for doped anatase and rutile TiO<sub>2</sub>. *J. Mol. Struct. Theochem.* **2003**, *626*, 271–277. [[CrossRef](#)]

24. Zhu, J.; Deng, Z.; Chen, F.; Zhang, J.; Chen, H.; Anpo, M.; Huang, J.; Zhang, L. Hydrothermal doping method for preparation of Cr<sup>3+</sup>-TiO<sub>2</sub> photocatalysts with concentration gradient distribution of Cr<sup>3+</sup>. *Appl. Catal. B Environ.* **2006**, *62*, 329–335. [[CrossRef](#)]
25. Tada, H.; Mitsui, T.; Kiyonaga, T.; Akita, T.; Tanaka, K. All-solid-state Z-scheme in CdS-Au-TiO<sub>2</sub> three-component nanojunction system. *Nat. Mater.* **2006**, *5*, 782–786. [[CrossRef](#)]
26. Ghosh, M.; Liu, J.; Chuang, S.S.C.; Jana, S.C. Fabrication of hierarchical V<sub>2</sub>O<sub>5</sub> nanorods on TiO<sub>2</sub> nanofibers and their enhanced photocatalytic activity under visible light. *ChemCatChem* **2018**, *10*, 3305–3318. [[CrossRef](#)]
27. Yang, J.; Zhang, J.; Zou, B.; Zhang, H.; Wang, J.; Schubert, U.; Rui, Y. Black SnO<sub>2</sub>-TiO<sub>2</sub> Nanocomposites with high dispersion for photocatalytic and photovoltaic applications. *ACS Appl. Nano Mater.* **2020**, *3*, 4265–4273. [[CrossRef](#)]
28. Zhang, L.; Yu, W.; Han, C.; Guo, J.; Zhang, Q.; Xie, H.; Shao, Q.; Sun, Z.; Guo, Z. Large scaled synthesis of heterostructured electrospun TiO<sub>2</sub>/SnO<sub>2</sub> nanofibers with an enhanced photocatalytic activity. *J. Electrochem. Soc.* **2017**, *164*, H651–H656. [[CrossRef](#)]
29. Li, J.J.; Weng, B.; Cai, S.C.; Chen, J.; Jia, H.P.; Xu, Y.J. Efficient promotion of charge transfer and separation in hydrogenated TiO<sub>2</sub>/WO<sub>3</sub> with rich surface-oxygen-vacancies for photodecomposition of gaseous toluene. *J. Hazard. Mater.* **2018**, *342*, 661–669. [[CrossRef](#)]
30. Chen, X.; Liu, L.; Yu, P.Y.; Mao, S.S. Increasing solar absorption for photocatalysis with black hydrogenated titanium dioxide nanocrystals. *Science* **2011**, *331*, 746–750. [[CrossRef](#)]
31. Kraeutler, B.; Bard, A.J. Heterogeneous photocatalytic preparation of supported catalysts. Photodeposition of platinum on TiO<sub>2</sub> powder and other substrates. *J. Am. Chem. Soc.* **1978**, *100*, 4317–4318. [[CrossRef](#)]
32. Sclafani, A.; Mozzanega, M.-N.; Pichat, P. Effect of silver deposits on the photocatalytic activity of titanium dioxide samples for the dehydrogenation or oxidation of 2-propanol. *J. Photochem. Photobiol. A Chem.* **1991**, *59*, 181–189. [[CrossRef](#)]
33. Disdier, J.; Herrmann, J.-M.; Pichat, P. Platinum/titanium dioxide catalysts. *J. Chem. Soc. Faraday Trans.* **1983**, *79*, 651–660. [[CrossRef](#)]
34. Kamat, P.V. Photochemistry on nonreactive and reactive (semiconductor) surfaces. *Chem. Rev.* **1993**, *93*, 267–300. [[CrossRef](#)]
35. Wang, C.Y.; Bahnemann, D.W.; Dohrmann, J.K. A novel preparation of iron-doped TiO<sub>2</sub> nanoparticles with enhanced photocatalytic activity. *Chem. Commun.* **2000**, 1539–1540. [[CrossRef](#)]
36. Zakeeruddin, S.M.; Nazeeruddin, M.K.; Humphry-Baker, R.; Péchy, P.; Quagliotto, P.; Barolo, C.; Viscardi, G.; Grätzel, M. Design, synthesis, and application of amphiphilic ruthenium polypyridyl photosensitizers in solar cells based on nanocrystalline TiO<sub>2</sub> films. *Langmuir* **2002**, *18*, 952–954. [[CrossRef](#)]
37. Bae, E.; Choi, W. Effect of the anchoring group (carboxylate vs phosphonate) in Ru-complex-sensitized TiO<sub>2</sub> on hydrogen production under visible light. *J. Phys. Chem. B* **2006**, *110*, 14792–14799. [[CrossRef](#)]
38. Park, H.; Choi, W. Effects of TiO<sub>2</sub> surface fluorination on photocatalytic reactions and photoelectrochemical behaviors. *J. Phys. Chem. B* **2004**, *108*, 4086–4093. [[CrossRef](#)]
39. Di Paola, A.; Marci, G.; Palmisano, L.; Schiavello, M.; Uosaki, K.; Ikeda, S.; Ohtani, B. Preparation of polycrystalline TiO<sub>2</sub> photocatalysts impregnated with various transition metal ions: Characterization and photocatalytic activity for the degradation of 4-nitrophenol. *J. Phys. Chem. B* **2002**, *106*, 637–645. [[CrossRef](#)]
40. Reszczyńska, J.; Grzyb, T.; Wei, Z.; Klein, M.; Kowalska, E.; Ohtani, B.; Zaleska-Medynska, A. Photocatalytic activity and luminescence properties of RE<sup>3+</sup>-TiO<sub>2</sub> nanocrystals prepared by sol-gel and hydrothermal methods. *Appl. Catal. B Environ.* **2016**, *181*, 825–837. [[CrossRef](#)]
41. Kusiak-Nejman, E.; Janus, M.; Grzmil, B.; Morawski, A.W. Methylene Blue decomposition under visible light irradiation in the presence of carbon-modified TiO<sub>2</sub> photocatalysts. *J. Photochem. Photobiol. A Chem.* **2011**, *226*, 68–72. [[CrossRef](#)]
42. Markowska-Szczupak, A.; Rokicka, P.; Wang, K.; Endo, M.; Morawski, A.; Kowalska, E. Photocatalytic water disinfection under solar irradiation by d-glucose-modified titania. *Catalysts* **2018**, *8*, 316. [[CrossRef](#)]
43. Wang, K.; Endo-Kimura, M.; Belchi, R.; Zhang, D.; Habert, A.; Bouclé, J.; Ohtani, B.; Kowalska, E.; Herlin-Boime, N. Carbon/graphene-modified titania with enhanced photocatalytic activity under UV and vis irradiation. *Materials* **2019**, *12*, 4158. [[CrossRef](#)] [[PubMed](#)]
44. Kowalska, E.; Mahaney, O.O.P.; Abe, R.; Ohtani, B. Visible-light-induced photocatalysis through surface plasmon excitation of gold on titania surfaces. *Phys. Chem. Chem. Phys.* **2010**, *12*, 2344–2355. [[CrossRef](#)]

45. Linic, S.; Christopher, P.; Ingram, D.B. Plasmonic-metal nanostructures for efficient conversion of solar to chemical energy. *Nat. Mater.* **2011**, *10*, 911–921. [[CrossRef](#)]
46. Tian, Y.; Tatsuma, T. Mechanisms and applications of plasmon-induced charge separation at TiO<sub>2</sub> films loaded with gold nanoparticles. *J. Am. Chem. Soc.* **2005**, *127*, 7632–7637. [[CrossRef](#)]
47. Raja-Mogan, T.; Ohtani, B.; Kowalska, E. Photonic crystals for plasmonic photocatalysis. *Catalysts* **2020**, *10*, 827. [[CrossRef](#)]
48. Rycenga, M.; Cobley, C.M.; Zeng, J.; Li, W.; Moran, C.H.; Zhang, Q.; Qin, D.; Xia, Y. Controlling the synthesis and assembly of silver nanostructures for plasmonic applications. *Chem. Rev.* **2011**, *111*, 3669–3712. [[CrossRef](#)]
49. Kazuma, E.; Yamaguchi, T.; Sakai, N.; Tatsuma, T. Growth behaviour and plasmon resonance properties of photocatalytically deposited Cu nanoparticles. *Nanoscale* **2011**, *3*, 3641–3645. [[CrossRef](#)]
50. El-sayed, M.A. Some interesting properties of metals confined in time and nanometer space of different shapes. *Acc. Chem. Res.* **2001**, *34*, 257–264. [[CrossRef](#)]
51. Burda, C.; Chen, X.; Narayanan, R.; El-Sayed, M.A. Chemistry and properties of nanocrystals of different shapes. *Chem. Rev.* **2005**, *105*, 1025–1102. [[CrossRef](#)] [[PubMed](#)]
52. Brus, L. Noble metal nanocrystals: Plasmon electron transfer photochemistry and single molecule raman spectroscopy. *Acc. Chem. Res.* **2008**, *41*, 1742–1749. [[CrossRef](#)] [[PubMed](#)]
53. Xia, Y.; Xiong, Y.; Lim, B.; Skrabalak, S.E. Shape-controlled synthesis of metal nanocrystals: Simple chemistry meets complex physics? *Angew. Chem. Int. Ed.* **2009**, *48*, 60–103. [[CrossRef](#)]
54. Kelly, K.L.; Coronado, E.; Zhao, L.L.; Schatz, G.C. The optical properties of metal nanoparticles: The influence of size, shape, and dielectric environment. *J. Phys. Chem. B* **2003**, *107*, 668–677. [[CrossRef](#)]
55. Hou, W.; Cronin, S.B. A review of surface plasmon resonance-enhanced photocatalysis. *Adv. Funct. Mater.* **2013**, *23*, 1612–1619. [[CrossRef](#)]
56. Evanoff, D.D.; Chumanov, G. Synthesis and optical properties of silver nanoparticles and arrays. *ChemPhysChem* **2005**, *6*, 1221–1231. [[CrossRef](#)]
57. Jain, P.K.; Huang, X.; El-Sayed, I.H.; El-Sayed, M.A. Noble metals on the nanoscale: Optical and photothermal properties and some applications in imaging, sensing, biology, and medicine. *Acc. Chem. Res.* **2008**, *41*, 1578–1586. [[CrossRef](#)]
58. Matsunaga, T.; Tomoda, R.; Nakajima, T.; Wake, H. Photoelectrochemical sterilization of microbial cells by semiconductor powders. *FEMS Microbiol. Lett.* **1985**, *29*, 211–214. [[CrossRef](#)]
59. Wolfrum, E.J.; Huang, J.; Blake, D.M.; Maness, P.C.; Huang, Z.; Fiest, J.; Jacoby, W.A. Photocatalytic oxidation of bacteria, bacterial and fungal spores, and model biofilm components to carbon dioxide on titanium dioxide-coated surfaces. *Environ. Sci. Technol.* **2002**, *36*, 3412–3419. [[CrossRef](#)]
60. Armon, R.; Weitch-Cohen, G.; Bettane, P. Disinfection of Bacillus spp. spores in drinking water by TiO<sub>2</sub> photocatalysis as a model for *Bacillus anthracis*. *Water Sci. Technol. Water Supply* **2004**, *4*, 7–14. [[CrossRef](#)]
61. Dillert, R.; Siemon, U.; Bahnemann, D. Photocatalytic disinfection of municipal wastewater. *Chem. Eng. Technol.* **1998**, *21*, 356–358. [[CrossRef](#)]
62. Wei, C.; Lin, W.Y.; Zainal, Z.; Williams, N.E.; Zhu, K.; Kruzlc, A.P.; Smith, R.L.; Rajeshwar, K. Bactericidal activity of TiO<sub>2</sub> photocatalyst in aqueous media: Toward a solar-assisted water disinfection system. *Environ. Sci. Technol.* **1994**, *28*, 934–938. [[CrossRef](#)] [[PubMed](#)]
63. Kim, B.; Kim, D.; Cho, D.; Cho, S. Bactericidal effect of TiO<sub>2</sub> photocatalyst on selected food-borne pathogenic bacteria. *Chemosphere* **2003**, *52*, 277–281. [[CrossRef](#)]
64. Wu, P.; Xie, R.; Imlay, K.; Shang, J.K. Monolithic ceramic foams for ultrafast photocatalytic inactivation of bacteria. *J. Am. Ceram. Soc.* **2009**, *92*, 1648–1654. [[CrossRef](#)]
65. Keller, V.; Keller, N.; Ledoux, M.J.; Lett, M.C. Biological agent inactivation in a flowing air stream by photocatalysis. *Chem. Commun.* **2005**, 2918–2920. [[CrossRef](#)]
66. Porley, V.; Chatzisyneon, E.; Meikap, B.C.; Ghosal, S.; Robertson, N. Field testing of low-cost titania-based photocatalysts for enhanced solar disinfection (SODIS) in rural India. *Environ. Sci. Water Res. Technol.* **2020**, *6*, 809–816. [[CrossRef](#)]
67. Hockberger, P.E. A History of ultraviolet photobiology for humans, animals and microorganisms. *Photochem. Photobiol.* **2002**, *76*, 561. [[CrossRef](#)]
68. Markowska-Szczupak, A.; Ulfig, K.; Morawski, A.W. The application of titanium dioxide for deactivation of bioparticulates: An overview. *Catal. Today* **2011**, *169*, 249–257. [[CrossRef](#)]

69. Sunada, K.; Minoshima, M.; Hashimoto, K. Highly efficient antiviral and antibacterial activities of solid-state cuprous compounds. *J. Hazard. Mater.* **2012**, *235*, 265–270. [[CrossRef](#)]
70. Deng, C.H.; Gong, J.L.; Zeng, G.M.; Zhang, P.; Song, B.; Zhang, X.G.; Liu, H.Y.; Huan, S.Y. Graphene sponge decorated with copper nanoparticles as a novel bactericidal filter for inactivation of *Escherichia coli*. *Chemosphere* **2017**, *184*, 347–357. [[CrossRef](#)]
71. Jafari, A.; Pourakbar, L.; Farhadi, K.; Mohamadgolizad, L.; Goosta, Y. Biological synthesis of silver nanoparticles and evaluation of antibacterial and antifungal properties of silver and copper nanoparticles. *Turkish J. Biol.* **2015**, *39*, 556–561. [[CrossRef](#)]
72. Qiu, X.; Miyauchi, M.; Sunada, K.; Minoshima, M.; Liu, M.; Lu, Y.; Li, D.; Shimodaira, Y.; Hosogi, Y.; Kuroda, Y.; et al. Hybrid Cu<sub>x</sub>O/TiO<sub>2</sub> nanocomposites as risk-reduction materials in indoor environments. *ACS Nano* **2012**, *6*, 1609–1618. [[CrossRef](#)] [[PubMed](#)]
73. Endo, M.; Janczarek, M.; Wei, Z.; Wang, K.; Markowska-Szczupak, A.; Ohtani, B.; Kowalska, E. Bactericidal properties of plasmonic photocatalysts composed of noble metal nanoparticles on faceted anatase titania. *J. Nanosci. Nanotechnol.* **2019**, *19*, 442–452. [[CrossRef](#)] [[PubMed](#)]
74. Ohtani, B.; Mahaney, O.O.P.; Amano, F.; Murakami, N.; Abe, R. What are titania photocatalysts?—An exploratory correlation of photocatalytic activity with structural and physical properties. *J. Adv. Oxid. Technol.* **2010**, *13*, 247–261. [[CrossRef](#)]
75. Nitta, A.; Takashima, M.; Takase, M.; Ohtani, B. Identification and characterization of titania photocatalyst powders using their energy-resolved distribution of electron traps as a fingerprint. *Catal. Today* **2019**, *321*, 2–8. [[CrossRef](#)]
76. Kowalska, E.; Wei, Z.; Karabiyik, B.; Herissan, A.; Janczarek, M.; Endo, M.; Markowska-Szczupak, A.; Remita, H.; Ohtani, B. Silver-modified titania with enhanced photocatalytic and antimicrobial properties under UV and visible light irradiation. *Catal. Today* **2015**, *252*, 136–142. [[CrossRef](#)]
77. Prieto-Mahaney, O.-O.; Murakami, N.; Abe, R.; Ohtani, B. Correlation between photocatalytic activities and structural and physical properties of titanium(IV) oxide powders. *Chem. Lett.* **2009**, *38*, 238–239. [[CrossRef](#)]
78. Kakuma, Y.; Nosaka, A.Y.; Nosaka, Y. Difference in TiO<sub>2</sub> photocatalytic mechanism between rutile and anatase studied by the detection of active oxygen and surface species in water. *Phys. Chem. Chem. Phys.* **2015**, *17*, 18691–18698. [[CrossRef](#)]
79. Buchalska, M.; Kobielski, M.; Matuszek, A.; Pacia, M.; Wojtyła, S.; Macyk, W. On oxygen activation at rutile-and anatase-TiO<sub>2</sub>. *ACS Catal.* **2015**, *5*, 7424–7431. [[CrossRef](#)]
80. Min, B.K.; Wallace, W.T.; Goodman, D.W. Support effects on the nucleation, growth, and morphology of gold nano-clusters. *Surf. Sci.* **2006**, *600*, L7–L11. [[CrossRef](#)]
81. Janczarek, M.; Wei, Z.; Endo, M.; Ohtani, B.; Kowalska, E. Silver- and copper-modified decahedral anatase titania particles as visible light-responsive plasmonic photocatalyst. *J. Photonics Energy* **2017**, *7*, 012008. [[CrossRef](#)]
82. DeSario, P.A.; Pietron, J.J.; Brintlinger, T.H.; McEntee, M.; Parker, J.F.; Baturina, O.; Stroud, R.M.; Rolison, D.R. Oxidation-stable plasmonic copper nanoparticles in photocatalytic TiO<sub>2</sub> nanoarchitectures. *Nanoscale* **2017**, *9*, 11720–11729. [[CrossRef](#)] [[PubMed](#)]
83. Wei, Z.; Janczarek, M.; Endo, M.; Wang, K.; Balcytis, A.; Nitta, A.; Méndez-medrano, M.G.; Colbeau-justin, C.; Juodkazis, S.; Ohtani, B.; et al. Noble metal-modified faceted anatase titania photocatalysts: Octahedron versus decahedron. *Appl. Catal. B Environ.* **2018**, *237*, 574–587. [[CrossRef](#)]
84. Banerjee, S.; Chakravorty, D. Optical absorption by nanoparticles of Cu<sub>2</sub>O. *Europhys. Lett.* **2000**, *52*, 468–473. [[CrossRef](#)]
85. Dias Filho, N.L. Adsorption of Cu(II) and Co(II) complexes on a silica gel surface chemically modified with 2-mercaptoimidazole. *Mikrochim. Acta* **1999**, *130*, 233–240. [[CrossRef](#)]
86. Irie, H.; Kamiya, K.; Shibamura, T.; Miura, S.; Tryk, D.A.; Yokoyama, T.; Hashimoto, K. Visible light-sensitive Cu(II)-grafted TiO<sub>2</sub> photocatalysts: Activities and X-ray absorption fine structure analyses. *J. Phys. Chem. C* **2009**, *113*, 10761–10766. [[CrossRef](#)]
87. Janczarek, M.; Endo, M.; Zhang, D.; Wang, K.; Kowalska, E. Enhanced photocatalytic and antimicrobial performance of cuprous oxide/titania: The effect of titania matrix. *Materials* **2018**, *11*, 2069. [[CrossRef](#)]
88. Endo-Kimura, M.; Janczarek, M.; Bielan, Z.; Zhang, D.; Wang, K.; Markowska-Szczupak, A.; Kowalska, E. Photocatalytic and antimicrobial properties of Ag<sub>2</sub>O/TiO<sub>2</sub> heterojunction. *ChemEngineering* **2019**, *3*, 3. [[CrossRef](#)]

89. Ikeda, S.; Sugiyama, N.; Pal, B.; Marci, G.; Palmisano, L.; Noguchi, H.; Uosaki, K.; Ohtani, B. Photocatalytic activity of transition-metal-loaded titanium(IV) oxide powders suspended in aqueous solutions: Correlation with electron-hole recombination kinetics. *Phys. Chem. Chem. Phys.* **2001**, *3*, 267–273. [[CrossRef](#)]
90. Janczarek, M.; Kowalska, E. On the origin of enhanced photocatalytic activity of copper-modified titania in the oxidative reaction systems. *Catalysts* **2017**, *7*, 317. [[CrossRef](#)]
91. Kowalska, E.; Abe, R.; Ohtani, B. Visible light-induced photocatalytic reaction of gold-modified titanium(IV) oxide particles: Action spectrum analysis. *Chem. Commun.* **2009**, 241–243. [[CrossRef](#)]
92. Kowalska, E.; Rau, S.; Ohtani, B. Plasmonic titania photocatalysts active under UV and visible-light irradiation: Influence of gold amount, size, and shape. *J. Nanotechnol.* **2012**, *2012*, 1–11. [[CrossRef](#)]
93. Zielińska-Jurek, A.; Kowalska, E.; Sobczak, J.W.; Lisowski, W.; Ohtani, B.; Zaleska, A. Preparation and characterization of monometallic (Au) and bimetallic (Ag/Au) modified-titania photocatalysts activated by visible light. *Appl. Catal. B Environ.* **2011**, *101*, 504–514. [[CrossRef](#)]
94. Wei, Z.; Rosa, L.; Wang, K.; Endo, M.; Juodkazis, S.; Ohtani, B.; Kowalska, E. Size-controlled gold nanoparticles on octahedral anatase particles as efficient plasmonic photocatalyst. *Appl. Catal. B Environ.* **2017**, *206*, 393–405. [[CrossRef](#)]
95. Méndez-Medrano, M.G.; Kowalska, E.; Ohtani, B.; Bahena Uribe, D.; Colbeau-Justin, C.; Rau, S.; Rodríguez-López, J.L.; Remita, H. Heterojunction of CuO nanoclusters with TiO<sub>2</sub> for photo-oxidation of organic compounds and for hydrogen production. *J. Chem. Phys.* **2020**, *153*, 034705. [[CrossRef](#)]
96. Werapun, U.; Pechwang, J. Synthesis and Antimicrobial Activity of Fe:TiO<sub>2</sub> Particles. *J. Nano Res.* **2019**, *56*, 28–38. [[CrossRef](#)]
97. Gurr, J.; Wang, A.S.S.; Chen, C.; Jan, K. Ultrafine titanium dioxide particles in the absence of photoactivation can induce oxidative damage to human bronchial epithelial cells. *Toxicology* **2005**, *213*, 66–73. [[CrossRef](#)]
98. Vargas, M.A.; Rodríguez-Páez, J.E. Facile Synthesis of TiO<sub>2</sub> Nanoparticles of different crystalline phases and evaluation of their antibacterial effect under dark conditions against *E. coli*. *J. Clust. Sci.* **2019**, *30*, 379–391. [[CrossRef](#)]
99. Endo-Kimura, M.; Kowalska, E. Plasmonic photocatalysts for microbiological applications. *Catalysts* **2020**, *10*, 824. [[CrossRef](#)]
100. Wang, M.; Zhao, Q.; Yang, H.; Shi, D.; Qian, J. Photocatalytic antibacterial properties of copper doped TiO<sub>2</sub> prepared by high-energy ball milling. *Ceram. Int.* **2020**, *46*, 16716–16724. [[CrossRef](#)]
101. Grass, G.; Rensing, C.; Solioz, M. Metallic copper as an antimicrobial surface. *Appl. Environ. Microbiol.* **2011**, *77*, 1541–1547. [[CrossRef](#)] [[PubMed](#)]
102. Mathew, S.; Ganguly, P.; Rhatigan, S.; Kumaravel, V.; Byrne, C.; Hinder, S.J.; Bartlett, J.; Nolan, M.; Pillai, S.C. Cu-Doped TiO<sub>2</sub>: Visible light assisted photocatalytic antimicrobial activity. *Appl. Sci.* **2018**, *8*, 2067. [[CrossRef](#)]
103. Miró-canturri, A.; Ayerbe-algaba, R.; Smani, Y. Drug repurposing for the treatment of bacterial and fungal infections. *Front. Microbiol.* **2019**, *10*, 41.
104. Markowska-Szczupak, A.; Wang, K.; Rokicka, P.; Endo, M.; Wei, Z.; Ohtani, B.; Morawski, A.W.; Kowalska, E. The effect of anatase and rutile crystallites isolated from titania P25 photocatalyst on growth of selected mould fungi. *J. Photochem. Photobiol. B Biol.* **2015**, *151*, 54–62. [[CrossRef](#)] [[PubMed](#)]
105. Eisenman, H.C.; Casadevall, A. Synthesis and assembly of fungal melanin. *Appl. Microbiol. Biotechnol.* **2015**, *93*, 931–940. [[CrossRef](#)]
106. Kühn, K.P.; Chaberny, I.F.; Massholder, K.; Stickler, M.; Benz, V.W.; Sonntag, H.G.; Erdinger, L. Disinfection of surfaces by photocatalytic oxidation with titanium dioxide and UVA light. *Chemosphere* **2003**, *53*, 71–77. [[CrossRef](#)]
107. Endo, M.; Wei, Z.; Wang, K.; Karabiyik, B.; Yoshiiri, K.; Rokicka, P.; Ohtani, B.; Markowska-Szczupak, A.; Kowalska, E. Noble metal-modified titania with visible-light activity for the decomposition of microorganisms. *Beilstein J. Nanotechnol.* **2018**, *9*, 829–841. [[CrossRef](#)]
108. Antsoegi-Uskola, M.; Markina-Iñarriraegui, A.; Ugalde, U. New insights into copper homeostasis in filamentous fungi. *Int. Microbiol.* **2020**, *23*, 65–73. [[CrossRef](#)]
109. Chen, F.; Yang, X.; Wu, Q. Antifungal capability of TiO<sub>2</sub> coated film on moist wood. *Build. Environ.* **2009**, *44*, 1088–1093. [[CrossRef](#)]
110. Markowska-Szczupak, A.; Ulfig, K.; Morawski, A.W. Antifungal effect of titanium dioxide, indoor light and the photocatalytic process in in vitro test on different media. *J. Adv. Oxid. Technol.* **2012**, *15*, 30–33. [[CrossRef](#)]

111. Meletiadis, J.; Meis, J.F.G.M.; Mouton, J.W. Analysis of growth characteristics of filamentous fungi in different nutrient media. *J. Clin. Microbiol.* **2001**, *39*, 478–484. [[CrossRef](#)] [[PubMed](#)]
112. Pombeiro-Sponchiado, S.R.; Sousa, G.S.; Andrade, J.C.R.; Lisboa, H.F.; Gonçalves, R.C.R. Production of melanin pigment by fungi and its biotechnological applications. In *Melanin*; Blumenberg, M., Ed.; InTechOpen: London, UK, 2017.
113. Carlile, M.J. The Photobiology of Fungi. *Annu. Rev. Plant. Physiol* **1965**, *16*, 175–202. [[CrossRef](#)]
114. Hill, E.P. Effect of light on growth and sporulation of *Aspergillus ornatus*. *J. Gen. Microbiol* **1976**, *95*, 39–44. [[CrossRef](#)] [[PubMed](#)]
115. Kopke, K.; Hoff, B.; Bloemendal, S.; Katschorowski, A.; Kamerewerd, J.; Kück, U. Members of the *Penicillium chrysogenum* velvet complex play functionally opposing roles in the regulation of penicillin biosynthesis and conidiation. *Eukaryot. Cell* **2013**, *12*, 299–310. [[CrossRef](#)] [[PubMed](#)]
116. Raffaini, G.; Ganazzoli, F. Molecular modelling of protein adsorption on the surface of titanium dioxide polymorphs. *Philos. Trans. R. Soc. A Math. Phys. Eng. Sci.* **2012**, *370*, 1444–1462. [[CrossRef](#)] [[PubMed](#)]
117. Liu, Q.; Zhang, Y.; Laskowski, J.S. The adsorption of polysaccharides onto mineral surfaces: An acid/base interaction. *Int. J. Miner. Process.* **2000**, *60*, 229–245. [[CrossRef](#)]
118. Topoglidis, E.; Cass, A.E.G.; Gilardi, G.; Sadeghi, S.; Beaumont, N.; Durrant, J.R. Protein adsorption on nanocrystalline TiO<sub>2</sub> films: An immobilization strategy for bioanalytical devices. *Anal. Chem.* **1998**, *70*, 5111–5113. [[CrossRef](#)]
119. Ellingsen, J.E. A study on the mechanism of protein adsorption to TiO<sub>2</sub>. *Biomaterials* **1991**, *12*, 593–596. [[CrossRef](#)]
120. Price, M.S.; Classen, J.J.; Payne, G.A. *Aspergillus niger* absorbs copper and zinc from swine wastewater. *Bioresour. Technol.* **2001**, *77*, 41–49. [[CrossRef](#)]
121. Markov, S.L.; Vidaković, A.M. Testing methods for antimicrobial activity of TiO<sub>2</sub> photocatalyst. *Acta Period. Technol.* **2014**, *45*, 141–152. [[CrossRef](#)]

**Publisher's Note:** MDPI stays neutral with regard to jurisdictional claims in published maps and institutional affiliations.



© 2020 by the authors. Licensee MDPI, Basel, Switzerland. This article is an open access article distributed under the terms and conditions of the Creative Commons Attribution (CC BY) license (<http://creativecommons.org/licenses/by/4.0/>).